X-RAY OBSERVATIONS OF ACCRETION POWERED PULSARS

A THESIS SUBMITTED TO
THE GRADUATE SCHOOL OF NATURAL AND APPLIED SCIENCES
OF
MIDDLE EAST TECHNICAL UNIVERSITY

BY

SITKI ÇAĞDAŞ İNAM

IN PARTIAL FULFILLMENT OF THE REQUIREMENTS FOR THE DEGREE OF

DOCTOR OF PHILOSOPHY

IN

PHYSICS

OCTOBER 2004

Approval of the Graduate School of Natural and Applied Sciences.

Prof. Dr. Canan Özgen
Director

I certify that this thesis satisfies all the requirements as a thesis for the degree of Doctor of Philosophy.

Prof. Dr. Sinan Bilikmen
Head of Department

This is to certify that we have read this thesis and that in our opinion it is fully adequate, in scope and quality, as a thesis for the degree of Doctor of Philosophy.

Prof. Dr. Altan Baykal
Supervisor

Examining Committee Members

Prof. Dr. Ali Alpar (SABANCI UNV.) _____

Prof. Dr. Altan Baykal (METU, PHYS) _____

Prof. Dr. Halil Kırbıyık (METU, PHYS) _____

Prof. Dr. Nilgün Kızıloğlu (METU, PHYS) _____

Prof. Dr. Ümit Kızıloğlu (METU, PHYS) _____

I hereby declare that all information in this document has been obtained and presented in accordance with academic rules and ethical conduct. I also declare that, as required by these rules and conduct, I have fully cited and referenced all material and results that are not original to this work.

Sıtkı Çağdaş İnam

ABSTRACT

X-RAY OBSERVATIONS OF ACCRETION POWERED PULSARS

İNAM, Sıtkı Çağdaş

PhD, Department of Physics

Supervisor: Prof. Dr. Altan Baykal

October 2004, 89 pages.

In this thesis, X-ray observations of four accretion powered pulsars are presented. Using RXTE observations of 4U 1907+09, we found three new pulse periods of the source. We found that the source spun-down almost at a constant rate of $\dot{\nu}$ = (-3.54 $\pm$0.02) $\times$ 10^{-14} Hz s^{-1} for more than 15 years. Using RXTE observations, X-ray flux related spectral and timing features in 2S 1417-62 were, in general, interpreted as a sign of a disc accretion with a similar geometry with a varying mass accretion rate, whereas spectral and timing features of the low X-ray flux regions were interpreted as a sign of possible temporary accretion geometry change prior to the next periastron. Using XMM-Newton and RXTE observations of SAX J2103.5+4545, we discovered quasi periodic oscillations around 0.044 Hz (22.7 sec) while the source was spinning-up with a rate of $(7.4 \pm 0.9) \times 10^{-13}$Hz s^{-1}. In the X-ray spectrum, we also found a soft component consistent with a blackbody emission with kT $\sim$ 1.9keV. Using RXTE observations, we also studied spectral evolution of Her X-1.

Keywords: Accretion powered pulsars, neutron stars, accretion disks, quasi periodic oscillations, x-ray binaries, x-ray spectrum

ÖZ

AKTARIM GÜÇLÜ ATARCALARIN X-IŞINI GÖZLEMLERİ

İNAM, Sıtkı Çağdaş
Doktora, Fizik Bölümü
Tez Yöneticisi: Prof. Dr. Altan Baykal

Ekim 2004, 89 sayfa.

Bu tezde dört aktarım güçlü atarcanın gözlemleri sunulmaktadır. 4U 1907+09'un gözlemlerini kullanarak kaynağın üç yeni atma periyodunu bulduk. Kaynağın hemen hemen sabit bir oranla, $\dot{\nu}$ = (-3.54 $\pm$0.02) $\times$ 10^{-14} Hz s^{-1}, 15 yıldan daha uzun süredir yavaşladığını da bulduk. XTE gözlemlerini kullanarak, genel olarak, 2S 1417-62'de x-ışınına bağlı tayfsal ve zamansal özellikler değişen kütle aktarım oranlı benzer geometri şekline sahip olan bir disk kütle aktarımının işareti olarak yorumlanırken düşük X-ışını akılı bölgelerin tayfsal ve zamansal özellikleri bir sonraki periastron öncesinde geçici kütle aktarım geometrisi değişimi olarak açıklandı. SAX J2103.5+4545'in XMM-Newton ve RXTE gözlemlerini kullanarak kaynağın $(7.4 \pm 0.9) \times 10^{-13}$Hz s^{-1} oranıyla hızlanırken 0.044 Hz civarında periodiğimsi salınımlar yaptığını keşfettik. Ayrıca X-ışını tayfında kT $\sim$ 1.9keV olan kara cisimle tutarlı yumuşak bir bileşke bulduk. RXTE gözlemlerini kullanarak, ayrıca Her X-1'in tayfsal evrimini de inceledik.

Anahtar Sözcükler: Aktarım güçlü atarcalar, nötron yıldızları, kütle aktarım diskleri, x-ışını çiftleri

ACKNOWLEDGMENTS

I would like to express my deepest gratitude to Prof. Dr. Altan Baykal for his guidance and insight throughout the research. I would also like to acknowledge Dr. D. Matthew Scott, Dr. Mark Finger and Dr. Jean Swank for their guidance.

I would also like to thank to Prof. Dr. Ali Alpar and Prof. Dr. Ümit Kızıloğlu for their helpful discussions and useful suggestions.

I thank my friends and colleagues in METU Astrophysics Group and NSSTC Gamma-ray Astronomy Group for their support. I especially would like to thank my wife and my parents for their moral support.

I acknowledge the Integrated Doctorate Program scholarship from the Scientific and Technical Research Council of Turkey (TÜBİTAK).

TABLE OF CONTENTS

PLAGIARISM iii

ABSTRACT iv

ÖZ v

ACKNOWLEDGMENTS vi

TABLE OF CONTENTS vii

CHAPTER

1 INTRODUCTION 1

2 OBSERVATIONAL PROPERTIES OF ACCRETION POWERED PULSARS 7

2.1 Pulse Profiles 7

2.2 Energy Spectra 12

2.3 Pulse Frequency Fluctuations 15

2.4 Quasi Periodic Oscillations 22

3 4U 1907+09 24

3.1 Introduction 24

3.2 Observations and Results 26

4 2S 1417-62 33

4.1 Introduction 33

4.2 Observations and Data Analysis 34

4.2.1 Timing Analysis 36

4.2.2 Spectral Analysis 38

4.3 Discussion and Conclusion 42

5 SAX J2103.5+4545 54
5.1 Introduction 54
5.2 Observations 56
5.2.1 RXTE 56
5.2.2 XMM 56
5.3 Data Analysis 57
5.3.1 Pulse Timing and Pulse profiles 57
5.3.2 Transient 22.7 sec QPO 60
5.3.3 Spectral Analysis 62
5.4 Discussion and Conclusion 66
5.4.1 QPO Feature of SAX J2103.5+4545 66
5.4.2 Blackbody and Iron Line Features of the Energy Spectrum 68

6 HER X-1 70
6.1 Introduction 70
6.2 Instruments and Observations 71
6.3 Spectral Analysis 72
6.4 Discussion and Conclusion 75

7 CONCLUSION 77

REFERENCES 80

LIST OF TABLES

2.1 Soft Blackbody components of Accretion Powered X-ray Binaries 14

3.1 Observation List for 4U 1907+09 27

3.2 RXTE Pulse Period Measurements of 4U 1907+09 29

3.3 Timing Solution of 4U 1907+09 for RXTE Observations[a] : 29

4.1 Observation List for 2S 1417-62 37

4.2 Spectral Parameters of PCA Observations of 2S 1417-62 38

4.3 Spectral Parameters of PCA-HEXTE Observations of the main outburst of 2S 1417-62 42

5.1 Spectral Models of SAX J2103.5+4545 64

6.1 Spectral Parameters of PCA Observations of Her X-1 72

LIST OF FIGURES

1.1 Spin period versus orbital period for the accretion powered pulsars with high mass companions (Chakrabarty 1996). 4

1.2 Distribution of accretion powered pulsars in galactic coordinates (Chakrabarty 1996). 5

2.1 Pulse profiles of GX 1+4 (White et al. 1983). 9

2.2 Pulse profiles of SMC X-1 (White et al. 1983). 9

2.3 Pulse profile of EXO 2030+375 as function of X-ray luminosity (Parmar, White and Stella 1989) 10

2.4 The logarithmic average power density estimators of angular accelerations of accreting powered pulsars together with two magnetar source (SGR 1900+14, SGR 1806-20) and two AXPs (1E 1048.1-5937, 1E 2259+59) and one rotation powered pulsar (Crab) as function of their X-ray luminosities. Note that Crab pulsar is one of the noisiest rotation powered pulsar (Baykal 2004). 17

3.1 Pulse period history of 4U 1907+09. 26

3.2 Pulse phase (Pulse Cycles) of 4U 1907+09 with respect to the constant pulse period of 440.5738 sec. 27

3.3 Pulse phase residuals of 4U 1907+09 with respect to the constant pulse period of 440.5738 sec after the derivative of pulse period 6.18×10^{-9} s s^{-1} is removed. 28

4.1 Background subtracted PCA count rate normalized to 5 PCUs in 3-20 keV band, frequency history before and after orbit subtraction are plotted against time. 5th degree polynomial fit to the orbit subtracted frequency history is overplotted. Initial time value corresponds to November 22, 1999, while the peak of the main outburst is about 50 days later than this date. Note that in some parts of the data, frequencies could not be estimated. These frequency values were left blank. All of the errors are in 1σ level. Vertical dashed lines indicate the orbital phase corresponding to periastron passages. 35

4.2 **(left)** Pulse fraction versus 3-20 keV unabsorbed X-ray flux. $(F_{max}-F_{min})/(F_{max}+F_{min})$ definition is used to calculate pulse fractions where F_{max} and F_{min} are the highest and lowest fluxes of the phase bins.**(middle)** Pulse Frequency Derivative versus 3-20 keV unabsorbed X-ray flux. Frequency derivatives were found by linear fitting of $\sim$ 20 day intervals of frequency history. X-ray fluxes were found by averaging the corresponding X-ray flux values. Solid line indicates best power law fit with the power index 1.01. **(right)** Pulse frequency derivative versus pulse fraction. Pulse frequency derivatives from the middle panel of this figure were plotted against pulse fractions which were found by averaging corresponding pulse fraction values. Errors in all of the panels are in 1σ level. 36

4.3 **(top to bottom)** Pulse profiles for days $\sim$ 31.2 (rise of the main-outburst), $\sim$ 50.6 (peak of the main outburst), $\sim$ 76.2 (peak of the main outburst at the second orbit), $\sim$ 95.3 (decline of the main outburst), $\sim$ 101.9 (low X-ray flux part), $\sim$ 107.1 (rise of the mini outburst), $\sim$ 124.1 (peak of the mini outburst), and $\sim$ 137.4 (decline of the mini outburst). Corresponding 3-20 keV unabsorbed fluxes in units 10^{-11}ergs.cm^2.s^{-1} are 75.1, 105.1, 54.0, 11.9, 1.18, 11.9, 21.9, and 3.69 respectively. Phases of the pulse profiles were manually aligned by using the similarities in the pulse shapes . . . 39

4.4 Combined PCA and HEXTE spectrum for the dataset 40070. The bottom panel shows the residuals of the fit in terms of σ values. . 40

4.5 Evolution of Hydrogen column density, Iron line complex peak energy, iron line equivalent width, power law index, power law normalization, cut-off energy, folding energy, and reduced χ^2. Vertical dashed lines indicate the orbital phase corresponding to periastron passages. 43

4.6 **(left)** Hydrogen column density as a function of 3-20 keV unabsorbed X-ray flux. **(right)** Power law index as a function of 3-20 keV unabsorbed X-ray flux. 44

5.1 Energy dependence of the pulse profiles of SAX J2103.5+4545. Pulse profiles were found by using EPIC-PN lightcurves that cover the energy ranges from top to bottom respectively. 59

5.2 **(top)** Power spectrum obtained from the 0.9-11.0 keV EPIC-PN lightcurve and rebinned by a factor of 4. QPO feature centered at 0.044 Hz is the prominent feature of the power spectrum. **(bottom)** Power spectrum rebinned by a factor of 8, multiplied by 2, and divided by the continuum fit consisting of a broken power law model with the power indices -0.34 ∓ 0.08 and -2.14 ∓ 0.05. Applying the method discussed by van der Klis (1989), significance of the QPO feature was calculated to be more than 6σ confidence level using the value of the peak at ~ 0.044 Hz as shown in this plot. 61

5.3 1-20 keV combined PN, MOS1, MOS2 and PCA spectrum of SAX J2103.5+4545 observed on January 6, 2003. The bottom panel shows the residuals of the fit in terms of σ values. 63

5.4 Spin phase dependence of 1-10 keV X-ray flux in units of 10^{-10} ergs s^{-1} cm^{-2}, Hydrogen column density in units of 10^{22} cm^{-2}, blackbody kT in units of keV, emission radius of the blackbody (assuming a source distance of 3.2 kpc) in units of km, photon index of the power law component of the spectral model, equivalent width of the iron line in units of eV, flux of the iron line in units of 10^{-13} ergs s^{-1} cm^{-2}, blackbody flux in units of 10^{-10} ergs s^{-1} cm^{-2}, power law flux in units of 10^{-10} ergs s^{-1} cm^{-2}, and reduced χ^2. All of the errors show 1σ confidence level. The spectral model used in fitting consists of an absorbed power law model with high energy cut-off, a soft blackbody component and an Iron line feature modeled as a Gaussian. The values of iron line peak energy, iron line sigma, cut-off and e-folding energies were found to be consistent with the constant values 6.42 keV, 0, 7.89 keV, and 27.1 keV respectively for all the spin phases, so these values were kept fixed while the values of the other model parameters were found. . 65

6.1 PCA count rate in units of cts/s, absorbed flux, unabsorbed flux, and power law flux in units of $10^{-10}\times$ ergs.cm^{-2}.s^{-1} in 3-20 keV energy range, unabsorbed flux / absorbed flux ratio, and reduced χ^2 as a function of time. Errors indicate 1σ confidence. 73

6.2 PCA count rate in units of cts/s, hydrogen column density in units of 10^{22} cm^2, partial covering fraction, iron line energy in units of keV, iron line flux in units of $10^{-11}\times$ ergs.cm^{-2}.s^{-1}, and iron line equivalent width in units of eV as a function of time. Errors indicate 1σ confidence. 74

CHAPTER 1

INTRODUCTION

An accretion powered pulsar is a rotating, highly magnetized neutron star accreting matter from its stellar companion. Due to the high magnetic fields nearby the neutron star's surface, accreting matter -being hot and therefore highly ionized- is channeled by the magnetic field lines onto the magnetic poles of the neutron star. When the matter falls onto the neutron star, it is rapidly decelerated at the magnetic poles, causing the release of the gravitational potential energy as X-ray emission from the magnetic poles. Due to the fact that the magnetic axis is in general tilted with respect to the spin axis of the neutron star, we may expect to see X-ray pulses from the neutron star if the resulting X-ray emission from one or both of the polar caps is in line with the observer.

The idea of formation of neutron stars arose from the calculations of Chandrasekhar (1931) and Landau (1932) which showed that the mass of a white dwarf cannot be indefinitely large. Beyond a certain mass limit, called *Chandrasekhar limit*, the pressure of a degenerate electron gas cannot sustain the gravitational pressure and the white dwarf star must collapse until the atomic nuclei come in contact and a giant atomic nucleus of size ~ 10 km is formed. After the discovery of the neutron in 1932 by Chadwick, in 1934, Baade and Zwicky suggested that

the supernova explosions are catastrophic processes of formation of stars consisting of neutrons. In 1968, the discovery of the radio pulsar at the center of the crab nebula (Hewish et al. 1968) was the first direct observational evidence of the existence of the neutron stars in our galaxy.

The first idea of the possibility of X-ray emission from compact stars was proposed by Zel'dovich and Guseynov (1966). After the discovery of an X-ray pulsar in the Crab nebula, *UHURU* observations of accretion pulsars led to the discovery of periodic X-ray pulsations from Cen X-3 (Giacconi et al. 1971b; Schreier et al. 1972) and Her X-1 (Tannanbaum et al. 1972). The origin of the pulsed emission was proposed to be fast rotating and highly magnetized ($B \geq 10^{11}$ G) neutron stars.

Much of our understanding of accretion powered pulsars comes from accurate timing of pulsed emission. We can obtain binary orbital parameters from the modulation in the observed pulse arrival times due to the orbital motion of the neutron star. Since a neutron star has a small moment of inertia ($I \sim 10^{45}$ kg.cm^2), we can also measure the changes in the pulsar spin frequency caused by the torques exerted by the accreted matter. Pulse frequency changes may yield important information about the nature of the accretion flow. A persistent spin-up or spin-down trend in the spin frequency indicates the presence of a persistent accretion disk (e.g. Baykal et al. 2002) while short term changes with no persistent trend is mostly an indication of a wind accretion or temporary accretion disk formation (e.g. Inam & Baykal 2000).

The binary systems with accretion powered pulsars can be classified into 3

groups according to the optical companions: 1. High mass X-ray binaries with OB supergiant companions, 2. Low mass X-ray binaries, 3. Be-star X-ray binaries.

Pulsars in high mass X-ray binaries with OB supergiant systems accrete mass either via persistent accretion disk due to Roche lobe overflow of their companions or via the stellar wind of their companions. Pulsars in high mass X-ray binaries with persistent accretion disks have usually shorter pulse periods and higher X-ray luminosities (SMC X-1 with the pulse period of 0.717s and luminosity of 6×10^{38} ergs.s^{-1}; Cen X-3 with the pulse period of 4.8s and luminosity of 8×10^{37} ergs.s^{-1}). Pulsars in high mass X-ray binaries that accrete mass via the stellar wind of their companions have usually longer periods and moderate X-ray luminosities (Vela X-1 with the pulse period of 283s and luminosity 6×10^{36} ergs.s^{-1} (Corbet, 1986; Chakrabarty, 1996).

Low mass X-ray binaries have late type or degenerate dwarf companions. These systems are steady and low luminosity X-ray sources ($< 10^{37}$ergs.s^{-1}). GX 1+4 and 4U 1626-67 are typical examples.

Systems with Be-star constitute the third group. These systems contain Be type companions which have dense equatorial winds. These systems are usually transient X-ray sources which are sometimes X-ray bright near the periastron passage of an eccentric orbit.

For the systems with high mass companions (OB supergiant or Be-star), we can roughly estimate the type of the system by plotting spin period versus orbital period (see Figure 1.1) which is also known as *Corbet diagram* (Corbet, 1986; Chakrabarty, 1996). For disk-fed supergiant systems, we have short spin and

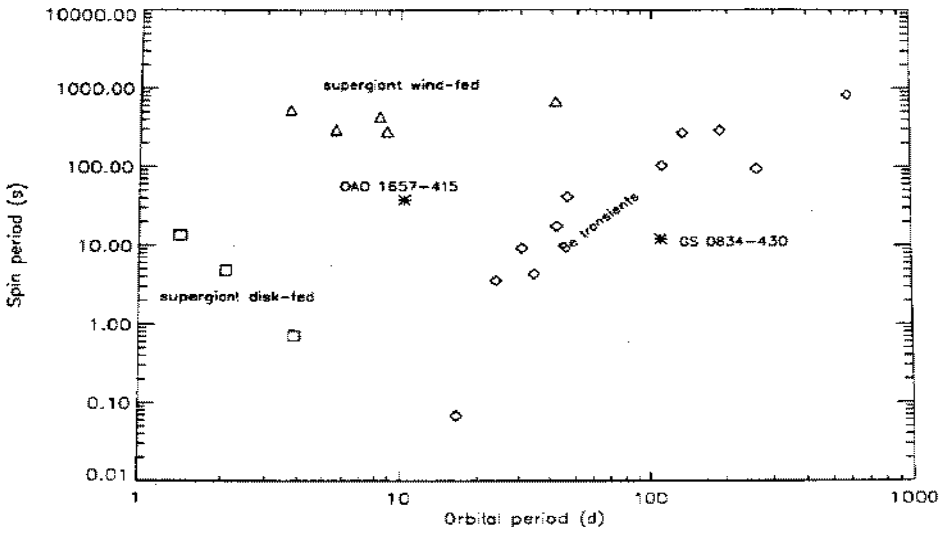

Figure 1.1: Spin period versus orbital period for the accretion powered pulsars with high mass companions (Chakrabarty 1996).

orbital periods. Short orbital period for such binary systems is the indication of smaller binary separation and therefore a greater possibility of Roche-lobe overflow of the companion resulting in the formation of persistent accretion disks around the neutron star. A Keplerian accretion disk is mostly expected to spin-up the neutron star which explains the short spin periods. For the wind-fed supergiant systems, spin and orbital periods are larger. Large orbital periods indicate larger binary separation, resulting in larger Roche lobe of the companion, so it is less likely to have Roche lobe overflow for this type of systems, making a stable accretion disk formation less likely. The pulsar accretes mass from the wind and no net trend of the accretion torque is expected which means that spin-up and spin-down torques should be similar in magnitude, excluding the possibility of a

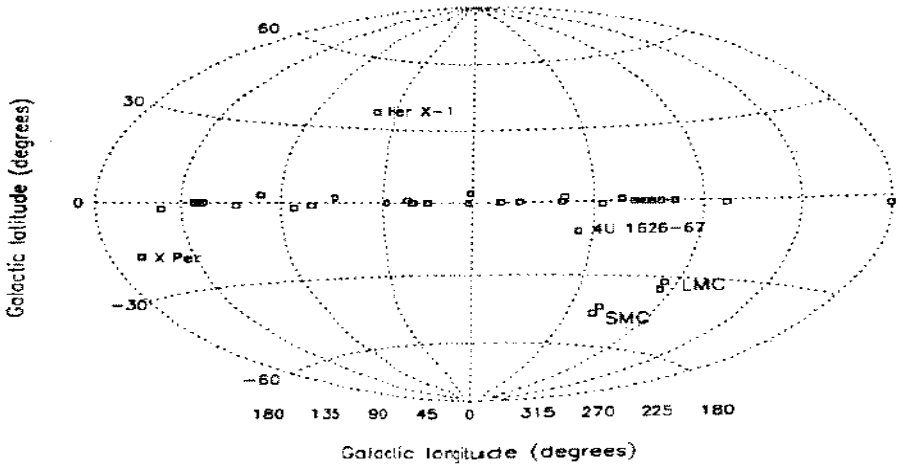

Figure 1.2: Distribution of accretion powered pulsars in galactic coordinates (Chakrabarty 1996).

spin-up trend and that is why we do not observe short spin periods from these systems. For systems with Be-star companions a correlation between orbital period and spin-period is observed (Corbet, 1986; Waters & van Kerkwijk 1989). This correlation trend is also plausible since the neutron stars in shorter orbital period systems are likely to accrete more material, and since neutron stars in such systems are likely to have temporary prograde accretion disks, we expect shorter spin periods for shorter orbital periods.

In Figure 1.2, we present distribution of accretion powered pulsars in the Galaxy. It is plausible to observe most of the accretion powered pulsars near galactic plane, because accretion powered pulsars should be the final stellar products of young high mass Population I main sequence stars which are mostly found

in low Galactic latitudes.

In this thesis, we use the datasets from observations of accretion powered pulsars 4U 1907+09, 2S 1417+62, SAX J2103.5+4545, and Her X-1 with *RXTE* (Rossi X-ray Timing Explorer) and *XMM-Newton* (X-ray Multi-Mirror Mission) observatories. The next chapter is a review about the fundamental observational properties of accretion powered pulsars. In Chapters 3 and 4, analysis of *RXTE* observations of 4U 1907+09 and 2S 1417+62 is presented. Chapter 5 is about timing and spectral results of our analysis of *RXTE* and *XMM-Newton* observations of SAX J 2103.5+4545. In Chapter 6, *RXTE* analysis of spectra of Her X-1 is presented. Results in Chapter 3 and 4 were published before in the Monthly Notices of the Royal Astronomical Society (Baykal et al. 2001; Inam et al. 2004a), while results in Chapter 5 were accepted for publication in the Astrophysical Journal (Inam et al. 2004b).

CHAPTER 2

OBSERVATIONAL PROPERTIES OF ACCRETION POWERED PULSARS

2.1 Pulse Profiles

Pulse profiles of accretion powered pulsars are one of the most important physical aspects to understand the physics of the accretion. The shapes of the pulses and the number of peaks in the pulse profiles depend on the location of the observer and the inclination between the rotation and the magnetic axes as well as the luminosity of the neutron star and the observed X-ray energy band.

Using the solutions of the one-dimensional hydrodynamic and radiative diffusion equations (Basko& Sunyaev, 1976; Wang& Frank, 1981), it is found that the outgoing radiation from the polar caps of the neutron star will not shock the inflowing gas stream below a limiting luminosity given by

$$L_{lim} \simeq 5 \times 10^{36} \frac{\sigma_T}{\sigma_s} r_5 R_6^{-1} M_{1.4} \mathrm{ergs.s}^{-1}, \tag{2.1}$$

where r_5, R_6, and $M_{1.4}$ are the radius of the accretion funnel in units of 10^5 cm, the radius and mass of the neutron star in units of 10^6 cm and $1.4 M_\odot$ respectively (White et al. 1983). In Equation 2.1, σ_s is the effective scattering cross section

of photons relative the Thomson value σ_T. σ_s depends basically on energy, polarization, and propagation angle of the photons relative to the field lines (Canuto, Lodenquai, & Ruderman 1971).

In case the X-ray luminosity of the accretion powered pulsar is below the luminosity given in Equation 2.1, outgoing radiation will not shock the inflowing gas stream which results in simpler (i.e. sinusoidal like) pulse profiles with little or no dependence on the photon energies. This case corresponds to the formation of *pencil beams* for which most of the radiation is emitted in the direction of the magnetic field lines. Pulse profiles of SAX J2103.5+4545 for which the luminosity is $\lesssim 10^{35}$ ergs.s^{-1} (see Chapter 5 and Inam et al. 2004b) may be an example of pencil beam formation.

If the X-ray luminosity of the accretion powered pulsar is above the limiting luminosity given in Equation 2.1, outgoing radiation shocks the inflowing gas stream and there will be a cylinder of emission above the neutron star corresponding to the shock region. In this case, we expect the photons with the energies close to the cyclotron resonance energy to escape in a *fan beam* for which most of the radiation is emitted perpendicularly to the magnetic field lines. In this case, we still expect to have sinusoidal like pulse profiles for the photon energies close to the cyclotron resonance energies. However, for the lower photon energies, we may either see the peak shifted by about 180° (as in the pulse profiles of GX 1+4 in Figure 2.1) possibly corresponding to the pencil beam emission or rather complex pulse profiles with more than three prominent peaks (as seen in the pulse profiles of SMC X-1 in Figure 2.1)

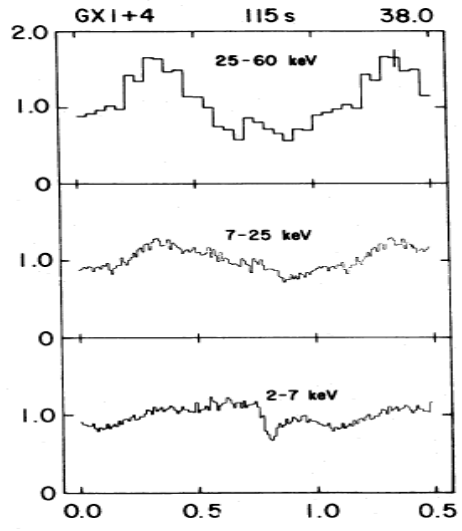

Figure 2.1: Pulse profiles of GX 1+4 (White et al. 1983).

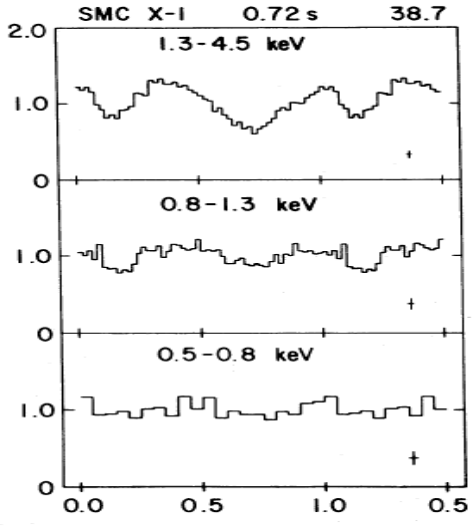

Figure 2.2: Pulse profiles of SMC X-1 (White et al. 1983).

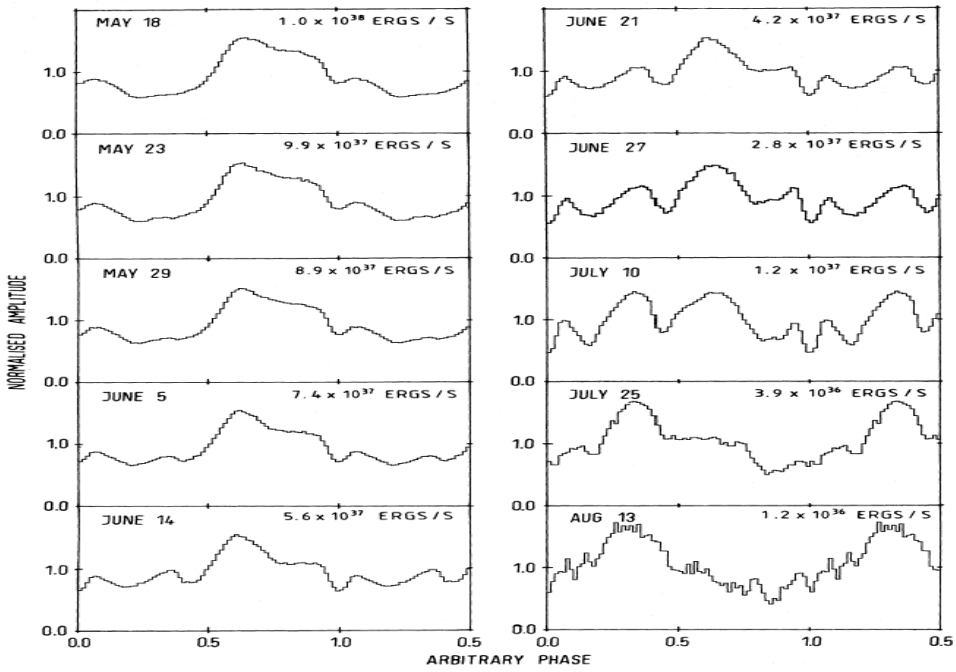

Figure 2.3: Pulse profile of EXO 2030+375 as function of X-ray luminosity (Parmar, White and Stella 1989)

A good example of pulse profiles' dependence on luminosity is the pulse profile variation of 42 seconds transient X-ray pulsar EXO 2030+375, for which the relative strength of the main pulse and interpulse changes when the outburst decays (Parmar, White and Stella 1989). This can occur if the beam pattern has changed phase by 180° and can be interpreted as a transition from fan beam to pencil beam (see Figure 2.3).

Accretion induced bursting pulsar GRO J1744-28 was initially discovered by BATSE (Kouveliotou et al. 1996). The pulse profile of 426 msec advanced ~ 25 msec during the burst (Stark et al. 1996). Both in quiescent and burst states X-ray luminosity of GRO J1744-28 was greater then 10^{37} erg sec^{-1} and the pulse profile was very similar in both states. Possible interpretation of phase shifts in

pulse arrival times is the shift of accretion footprint during the burst. Therefore the fan beam is shifted with respect to the observer line of sight during the burst.

From the discussion above for pencil and fan beams, pulse profiles of accretion powered pulsars tend to be sinusoidal like for all photon energies except for the low energy bands corresponding to the energies below cyclotron resonance energy of the high luminosity accretion powered pulsars (i.e. pulsars with luminosities greater than the luminosity given by Equation 2.1). This sinusoidal like pulse profiles of the accretion powered pulsars have always been observed to have either one or two pulse peaks except some minor structures (Bulik et al. 2003; Bildsten et al. 1997; Nagase, 1989). Assuming that an accreting neutron star has a pure centered dipole magnetic field, the geometry of accretion powered pulsars can be described with two angles: θ, the angle between the rotation axis and direction to the observer, and β, the angle between the magnetic and rotation axis. Then, the single pulse peak, corresponding to the case when only one magnetic polar cap is seen, is observed when

$$\theta < 90^\circ - \beta - \delta_g, \tag{2.2}$$

where δ_g is the gravitational light deflection of a photon emitted parallel to the surface of the neutron star with the assumption that the magnetic beaming is not very strong and that there are X-ray photons emitted parallel to the surface of the neutron star. In the Newtonian case ($\delta_g = 0^\circ$), if the angles β and θ are chosen randomly, the fraction of single pulsed objects is found to be $\simeq 0.214$ (Bulik et al. 2003).

The angles β and θ also determine the number of pulse peaks in the pulse profiles within the fan beam model (Bulik et al. 2003). For the case when there are two accretion columns radiating with constant specific intensity, the beam will be a function of the angle ψ only, which is the angle between the magnetic axis and the direction to the observer. It is interesting to note that the fan beam model predicts triple and quadruple pulse peaks as well as single and double pulse peaks. However, the observations of the accretion powered pulsars have not yielded triple and quadruple pulse peaks except for the pulse profiles obtained from lower energy bands of high luminosity pulsars where the fan beam model is not applicable.

2.2 Energy Spectra

Energy spectra of the accretion powered pulsars can be regarded as another important indicator of physics in the vicinity of the mass accreting neutron stars.

In the simplest consideration, we consider that the luminosity of an accretion powered pulsar which is accreting plasma from either wind or an accretion disk can approximately be written as

$$L \simeq \frac{GM\dot{M}}{R}, \tag{2.3}$$

where G is the gravitation constant, M is the mass of the neutron star, $\dot{M}$ is the mass accretion rate and R is the radius of the neutron star. When writing Equation 2.3, we assume that whole gravitational energy release of the accreting plasma is converted as the source of the electromagnetic radiation of the neutron

star.

If we further assume that the resultant spectrum of the neutron star is similar to that of a blackbody (as for many astronomical objects, e.g. main sequence stars), we equate the accretion luminosity with the blackbody luminosity ($A_{cap}\sigma T^4$, where A_{cap} is the polar cap area (~ 1 km^2), which is a small fraction of the total surface of the neutron star, σ is Stefan-Boltzmann constant and T is the blackbody temperature). For typical accretion powered pulsar luminosities ($\sim 10^{36}$ ergs/s), blackbody temperature is found to be $\sim 3.5 \times 10^7$K. Using Wien's displacement law, we expect to have a peak in the blackbody temperature at photon energies of about ~ 2.5 keV. Even though this value is comparable to the peak of X-ray spectra of accretion powered X-ray pulsars, the observed X-ray spectra are much harder than a blackbody and have been represented by a various models. Most commonly model consist of a power law with an high energy cutoff (White et al. 1983, Mihara 1995, Coburn et al., 2002). In these models, overall continuum can be represented as,

$$f(E) = AE^{-\Gamma}, \qquad E \leq E_{cut} \tag{2.4}$$

$$f(E) = AE^{-\Gamma} e^{(E_{cut}-E)/E_{fold}}, \qquad E \geq E_{cut}, \tag{2.5}$$

where Γ is the power law index varying, E_{cut} is the high energy cut off, and E_{fold} is e-folding energy.

In the spectra of some of the accretion powered pulsars, soft blackbody component has been observed. This soft component can be interpreted either as an emission from polar cap or an emission from accretion disk and in some cases as

Table 2.1: Soft Blackbody components of Accretion Powered X-ray Binaries (Baykal 2004)

Name	kT (keV)	Emis.Rad. (km)	References
Polar Cap Interpretation:			
EXO 2030+375	$\sim$ 1.1 - 1.3	$\sim$1-6	Reig and Coe 1999
SAX J1808.4-3658	$\sim$0.5-0.8	$\sim$ 3	Gierlinski et al. 2002
XTE J0920-314	$\sim$ 0.7	$\sim$ 5-8	Juett et al. 2003
SAX J2103.5+4545	$\sim$1.9	$\sim$ 0.4	Inam et al. 2004b
Emission from accretion disk or the surrounding material:			
Her X-1	0.16-0.17		Endo et al. 2000
Cen X-3	$\sim$ 0.1		Burderi et al. 2000
SMC X-1	0.13-0.15		Paul et al. 2002
LMC X-4	$\sim$ 0.17		Paul et al. 2002

a reprocessed emission from the surrounding material (Table 2.1)

Surface magnetic fields of a pulsar can be inferred from the cyclotron resonance scattering feature (CRSF), commonly called "cyclotron lines". These line like spectral feature arises as a result of the resonant scattering of photons by electrons whose energies are quantized into Landau levels by strong magnetic field (Meszaros 1992). The fundamental energy at which CRSF observed is given as

$$E_c = 11.6 \frac{B}{10^{12} G} (1+z)^{-1} keV, \tag{2.6}$$

where B is the magnetic field in the scattering region and z is the gravitational red shift. The quantized energy levels of the electrons are harmonically spaced at E_c, $2E_c$, $3E_c$, etc.. At sufficiently high magnetic fields ($E_c > 35$ keV), relativistic effects become important.

The first detection of CRSF was made by Trumper et al., (1978) from Her X-1 at $\sim$ 40 keV. In a recent paper by Coburn et al. (2002), the theory and observations of CRSFs in accretion powered pulsars were discussed in details.

2.3 Pulse Frequency Fluctuations

Pulse frequency fluctuations in accreting neutron stars originate both outside and inside the object. The external torques is due to the angular momenta carried by the accretion flow while the internal torques depend on the coupling between the superfluid interior and the solid outer crust. In general, external fluctuations of the torque are filtered by the coupling between the crust and superfluid interior to produce output represented by observed changes in the angular velocity (Lamb, Pines and Shaham 1978a,b, Deeter and Boynton 1982). In order to estimate the type of noise processes and core superfluidity, techniques were developed by Deeter (1984) and Cordes (1980) for the estimation of red noise power density and associated random walk noise strengths (see also Scott, Finger and Wilson 2003, Erkoca 2004).

If we assume that the noise process consists of individual torque events followed by neutron star's response by $\delta\Omega(t - t_i)$ and that these events occur at random times t_i and at a rate R such that during interval T, the number of events obeys a Poisson distribution with mean value RT, and the times t_i are uniformly distributed for $0 \leq t_i \leq T$ then angular velocity fluctuations of the crust can be written in terms of individual events,

$$\Delta\Omega = \sum_{i=1}^{K} \delta\Omega(t - t_i) \tag{2.7}$$

in the form of shot noise (Rice 1954). Then the power spectrum of the noise in the $\Delta\Omega$,

$$P_{(\Delta\omega)} = R|g(\omega)|^2, \tag{2.8}$$

where $g(\omega) = \int \delta\Omega(t) e^{i\omega t} dt$ is the Fourier transform of the individual shot.

For the r(=1,2...)th time integral of white noise time series (or rth order red noise) with strength S_r, the mean square residual for data spanning an interval T is given by (Rice 1954),

$$< \Delta\Omega^2 >= S_r T^{2r-1}, \tag{2.9}$$

where Ω is the variation in angular velocity of the neutron star and the noise strength $S_r = R < \delta\Omega^2 >$ can be expressed in terms of rate of the events R times rms step size of angular velocities $< \delta\Omega^2 >$.

Noise strengths S_r in time domain are related by power spectra in the following form

$$P_\Omega = S_r (2\pi f)^{-2r}. \tag{2.10}$$

For r=1 case, relation between power spectra of angular acceleration fluctuations and angular velocity fluctuations can be expressed as (Boynton 1981),

$$P_{\dot{\Omega}} = (2\pi f)^2 P_\Omega = S_{r=1}. \tag{2.11}$$

In Figure 2.4, the rotational noise strengths of accreting powered pulsars as a function of their X-ray luminosities is shown. In order to compare magnitudes of noise strengths with other classes of neutron stars noise strengths of two magnetar (SGR 1900+14, SGR 1806-20) and two AXPs (1E 1048.1-5937, 1E 2259+59) and one rotation powered pulsar (Crab) are included.

The short term pulse frequency fluctuations can be approximated with a two component neutron star model (Baym et al., 1969). In this model, one component

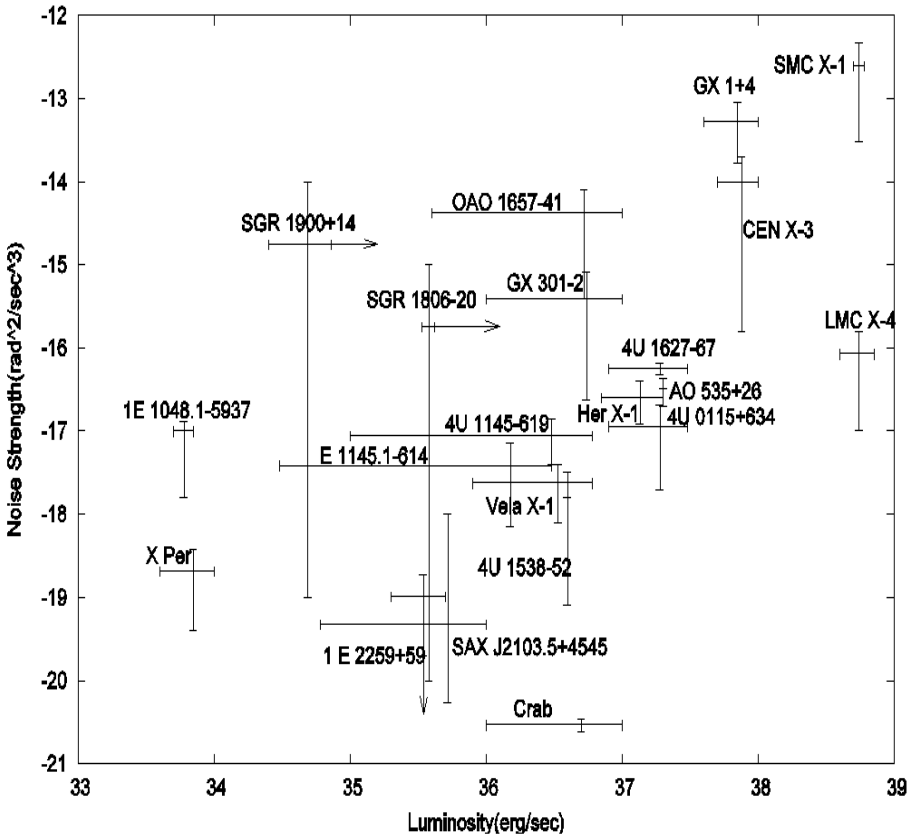

Figure 2.4: The logarithmic average power density estimators of angular accelerations of accreting powered pulsars together with two magnetar source (SGR 1900+14, SGR 1806-20) and two AXPs (1E 1048.1-5937, 1E 2259+59) and one rotation powered pulsar (Crab) as function of their X-ray luminosities. Note that Crab pulsar is one of the noisiest rotation powered pulsar (Baykal 2004).

is the crust charged particle system consisting of protons, electrons and the crust with inertia I_c which rotates with angular velocity Ω_c. The second component is the core neutron superfluid, with moment of inertia I_s, which rotates with angular velocity Ω_s. Any external torque on the crust creates a lag between Ω_c and Ω_s. The two components are coupled by crust core coupling time τ,

$$I_c\dot{\Omega}_c = N(t) - \frac{I_c}{\tau}(\Omega_c - \Omega_s), \tag{2.12}$$

$$I_s\dot{\Omega}_s = \frac{I_c}{\tau}(\Omega_c - \Omega_s), \tag{2.13}$$

where N(t) is the external torque exerted on the neutron star as a function of time t..

The torque on the neutron star ($\tau << T_m$, where T_m is the torque measuring time) can be written in terms of specific angular momentum (l) added to neutron star at some radius with a certain mass accretion rate (Lamb 1991).

$$I\dot{\Omega} = \dot{M}l. \tag{2.14}$$

If the accretion is from a Keplerian disk (Ghosh and Lamb 1979a,b) then we can write the external torque as

$$I\dot{\Omega} = n(\omega_s)\dot{M}l_K, \tag{2.15}$$

where $l_K = (GMr_0)^{1/2}$ is the specific angular momentum added by a Keplerian disk to the neutron star at the inner disk edge $r_0 \approx 0.5r_A$ ($r_A = (2GM)^{-1/7}\mu^{4/7}\dot{M}^{-2/7}$ being the Alfven radius), μ ($\sim BR^3$ where B and R are the surface magnetic field and radius of the neutron star) is the neutron star magnetic moment. $n(w_s) \approx 1.4(1 - \omega_s/\omega_c)/(1 - \omega_s)$ is called *dimensionless torque* as it measures

the variation of the accretion torque as functions of fastness parameter (ω_s) and the critical fastness parameter (ω_c). In this context, fastness parameter can be defined as

$$w_s = \Omega/\Omega_K(r_o) = 2\pi P^{-1} G^{-1/2} M^{-5/7} \mu^{6/7} \dot{M}^{-3/7}, \tag{2.16}$$

and w_c is the critical value of this parameter for which the accretion torque is expected to vanish ($w_c \sim 0.35 - 0.85$ depending on the electrodynamics of the disk, Lamb 1989).

In the model by Ghosh and Lamb (1979b), the torque experienced by the neutron star will cause a spin-up if the neutron star is a slow rotator ($w_s < w_c$) and the accretion disk rotates in the same sense with the spin direction of the neutron star. If the accretion disk rotates in the opposite direction with the spin direction of the neutron in the slow rotator case , we expect to the neutron star to spin-down (see Lamb 1991). Even if the neutron star is rotating in the same sense as the disk flow, the torque will spin-down if it is rotating too rapidly ($w_c \lesssim w_s$). This model also predicts positive correlation between angular acceleration ($\dot{\Omega}$) and mass accretion rate ($\dot{M}$) if the disk is rotating in the same sense as the neutron star.

For the accretion when there is no persistent accretion disk, observations show that the simple model consisting of accretion from a spherically symmetric wind is not a complete description of high mass X-ray binaries with wind accretion (Blondin et al. 1990 and references therein).

From the hydrodynamic simulations, it is seen that stellar wind is disrupted in the vicinity of a compact X-ray source (a neutron star for our case) which causes plasma to lose its homogeneity. The interaction of the incident flow with the shock fronts in the vicinity of the neutron star can produce temporary accretion disks (Taam& Fryxell 1988, 1989; Blondin et al. 1990). Formation of prograde disk is the only possibility if there is large asymmetries in the wind (i.e. with density inhomogeneities of scale length comparable to or smaller than the accretion radius). For the case of smaller asymmetries, interaction of the plasma with the shock fronts can produce disks which circulate in prograde and retrograde directions.

Using the results of the numerical studies of wind accretion, these points can be inferred:

1. We expect no correlation between the torque exerted on the neutron star and X-ray flux. Accretion from wind does not lead to the formation of a stable disk, so we do not expect to find such a correlation for an accretion powered pulsar accreting from its companion's stellar wind.

2.We expect to find a correlation between specific angular momentum (l and torque. Correlation of specific angular momentum and torque for negative and positive torques shows that there is temporary accretion disk formation in both prograde and retrograde directions without a considerable change in mass accretion which can be seen from Equation 2.14 for which $l = l_K = \pm(GMr_0)^{1/2}$ is the specific angular momentum obtained from the inner boundary of the disk. For the near zero values of the torque, our specific angular momentum is also near

zero which shows us that the accretion flow is radial.

3. When a temporary accretion disk forms around the neutron star, we expect an increase in specific angular momentum and decrease in mass accretion rate. This is because of the fact that plasma accumulates in the disk and rotates around the neutron star with near Keplerian velocities causing a lag in the fall of the plasma onto the neutron star's surface.. Thus, if we can find time intervals with high specific angular momentum and low mass accretion rate, we can say that accretion disk formation is probable for these intervals.

4. When the disk alternates its sense of rotation, we expect an increase in mass accretion rate. For this case, rotating disk is disrupted and plasma begins to fall radially on to the neutron star's surface causing an increase in mass accretion rate.

Even if the disk accretion is present, it was suggested by van Kerkwijk et al., (1998) that torque reversals observed in some of the accretion powered pulsars is possible and due to the disk being warped to such an extent that the inner region becomes tilted by more than 90 degrees. This means that the inner region of the disk becomes retrograde, leading a negative torque.

Generally persistent accreting sources (i.e. Her X-1, Cen X-3, Vela X-1, OAO 1657-415, GX 301-2, 4U 1626-67, 4U 1538-52, GX 1+4) do not show correlation between spin rate and luminosity (Bildsten et al. 1997; Inam and Baykal 2000). During the outbursts, transient accreting pulsars show correlation between accretion torque and luminosity. These sources are EXO 2030+375 (Parmar et al., 1989), 2S 1417-62 (Finger, Wilson, Chakrabarty 1996, Inam et al.,

2004), AO535+26 (Finger, Wilson, Harmon 1996), GRO J1744-28 (Bildsten et al., 1997), XTE J1543-568 (Int't Zand, Corbet and Marshall 2001), SAX J2103+4545 (Baykal, Stark and Swank 2002), KS 1947+300 (Galloway, Morgan and Levine 2004).

2.4 Quasi Periodic Oscillations

Quasi periodic oscillations in the X-ray band having periods in the range of 10-400 mHz have been observed in many accretion powered X-ray pulsars: 4U 0115+63 (Soong and Swank 1989), EXO 2030+375 (Angelini, Stella and Parmar 1989), 4U 1626-67 (Shinoda, Kii and Mitsuda 1990), SMC X-1 (Angelini, Stella and White 1991), V0332+53 (Takeshima, Dotani and Mitsuda 1994), AO535+262 (Finger, Wilson and Harmon 1996), GRO J1744-28 (Zhang, Morgan and Jahoda, 1996), X Per (Takeshima 1997), 4U 1907+09 (In't Zand, Baykal and Strohmayer 1998a), XTE J1858+034 (Paul and Rao 1998), LMC X-4 (Moon and Eikenberry 2001a), Her X-1 (Moon and Eikenberry 2001b), SAX J2103.5+4545 (Inam et al., 2004). Models that explain the QPO phenomenon in accretion powered X-ray pulsars fall basically into three categories: Keplerian frequency model explains QPOs as being produced due to some inhomogeneities at the inner edge of the Keplerian disk (r_0) which modulate the lightcurve at the Keplerian frequency $\nu_{QPO} = \nu_K$ (van der Klis et al., 1987). In the beat frequency model, the accretion flow onto the neutron star is modulated at the beat frequency between the Keplerian frequency at the inner edge of the accretion disk and the neutron star spin frequency $\nu_{QPO} = \nu_K - \nu_s$ (Alpar and Shaham 1985). The third model involves

accretion flow instabilities (Fronter et al., 1989, Lamb 1988), and applies only to the sources that have luminosities close to Eddington limit.

CHAPTER 3

4U 1907+09

3.1 Introduction

4U 1907+09 is an accretion powered X-ray binary pulsar which is accreting plasma from a blue supergiant companion star. It was discovered as an X-ray source by Giacconi et al. (1971) and has been studied using instruments on board Ariel V (Marshall & Ricketts 1980), Tenma (Makishima et al., 1984), EXOSAT (Cook & Page 1987), Ginga (Makishima & Mihara 1992, Mihara 1995), and RXTE (In 't Zand, Strohmayer & Baykal 1997, In 't Zand, Baykal & Strohmayer 1998, In 't Zand, Strohmayer & Baykal 1998). Marshall & Ricketts (1980) first determined the orbital period of the binary at 8.38 days by analyzing the data taken between 1974 and 1980 from a survey instrument on board Ariel V. Folding the light curve of these data, they found two flares, a primary and a secondary, each occurring at the same orbital phase. Subsequent Tenma observations of this source have shown a pulse period at 437.5 sec (Maksihima et al., 1984). Later EXOSAT (Cook & Page 1987) and recent RXTE observations (In 't Zand, Baykal & Strohmayer 1998, In 't Zand, Strohmayer & Baykal 1998) have shown that these flares are locked to orbital phases separated by half an orbital period. Makishima et al., (1984) and Cook & Page (1987) suggested that the two flares

are due to an equatorial disk-like envelope around a companion star which is inclined with respect to the orbital plane. When the neutron star crosses the disk, the mass accretion rate onto the neutron star, therefore the X-ray flux, increases temporarily. Transient $\sim$ 18 sec oscillations have appeared during the secondary flare (In 't Zand, Baykal & Strohmayer 1998). These oscillations may be interpreted as Keplerian motion of an accretion disk near the magnetospheric radius. Due to the long spin period the co-rotation radius is much larger than the magnetospheric radius corresponding to the magnetic field of 2.1×10^{12} Gauss implied by a cyclotron feature in the X-ray spectrum (Cusumano et al., 1998). Therefore 4U 1907+09 is not likely to be spinning near equilibrium, unlike other accretion powered X-ray pulsars. The 18 second quasi periodic oscillation at the flare suggests the formation of transient accretion disks from the wind accretion (In 't Zand, Baykal & Strohmayer 1998). Another interesting feature of the source is the sudden decrease in X-ray intensity by a factor of $\sim 10^2$, during time intervals ranging from a few minutes to $\sim$ 1.5 hour (In 't Zand, Strohmayer & Baykal 1997). The spectra at the dipping activity and outside the dip periods were similar with no indication of large changes in the column density of cold circumstellar matter (i.e. N_H remains below 10^{23} cm^{-2}). It is suggested that the mass accretion rate ceased due to the inhomogeneous spherical wind from the companion.

In this chapter, we have investigated the stability of the spin down rate. This source has shown spin down rate changes less than $\sim$ 8 % within 12 years (In 't Zand, Strohmayer & Baykal 1998). Using the archival RXTE observations,

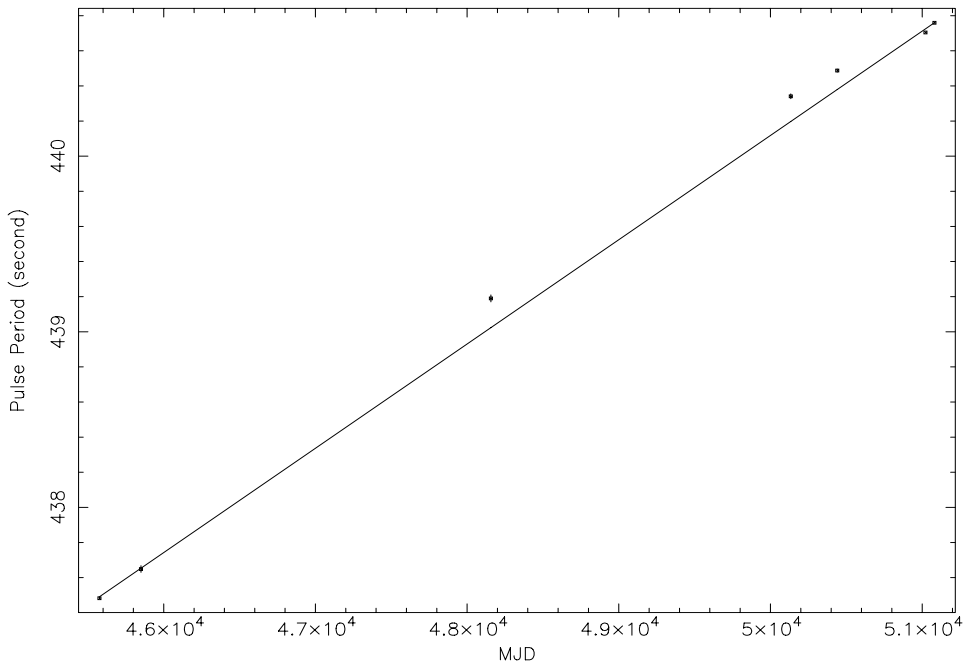

Figure 3.1: Pulse period history of 4U 1907+09.

we measured three new pulse periods covering a time span of over 2 years in addition to the previous four pulse period measurements. With $\sim 10^3 - 10^4$ sec observations separated by intervals of the order of a month we have been able to connect the pulses in phase and to construct the timing solution extending over a year. The residuals of pulse arrival times yielded a very low noise strength. Our findings imply that the source has a very stable spin down rate even over short time intervals, in contrast to the noise seen in other HMXRBs.

3.2 Observations and Results

The observations used in this chapter are listed in Table 3.1. The results presented here are based on data collected with the Proportional Counter Array

Table 3.1: Observation List for 4U 1907+09

Time of Observation day/month/year	Exposure sec
25/11/1996	9163
19-27/12/1996	35102
29/01/1997	849
19/03/1997	7430
29/04/1997	13908
26/05/1997	8352
18/06/1997	11695
17/07/1997	724
24/08/1997	6976
23/09/1997	5811
18/10/1997	7913
17/11/1997	7787
14/12/1997	645
26-29/07/1998	33211
18/09-01/10/1998	175382

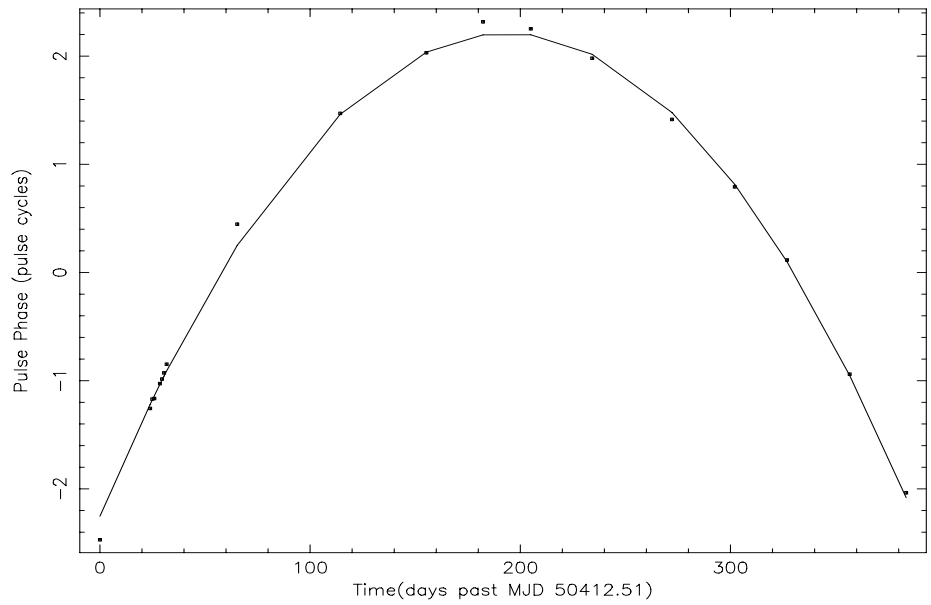

Figure 3.2: Pulse phase (Pulse Cycles) of 4U 1907+09 with respect to the constant pulse period of 440.5738 sec.

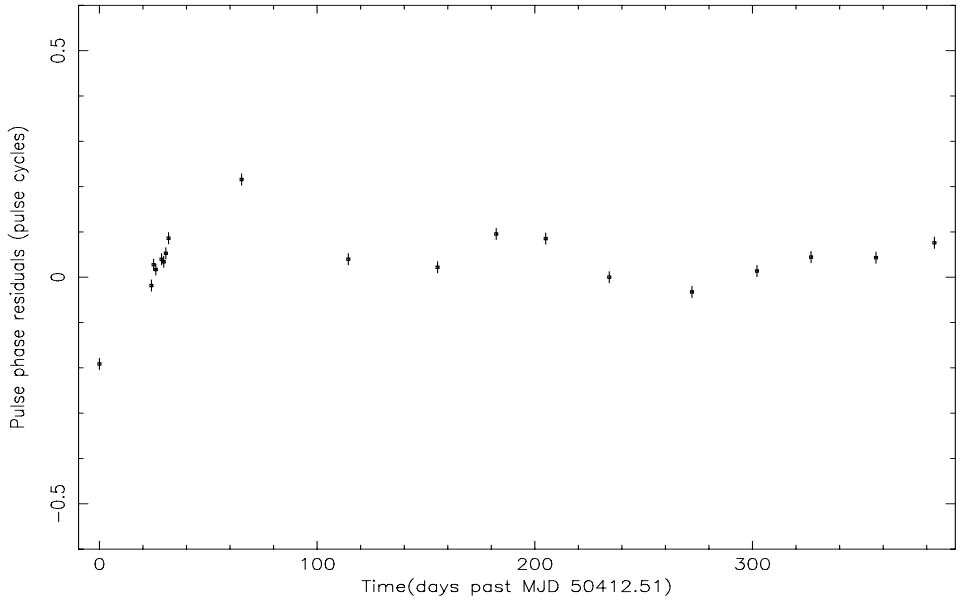

Figure 3.3: Pulse phase residuals of 4U 1907+09 with respect to the constant pulse period of 440.5738 sec after the derivative of pulse period 6.18×10^{-9} s s^{-1} is removed.

(PCA, Jahoda et al., 1996). The PCA instrument consists of an array of 5 proportional counters operating in the 2-60 keV energy range, with a total effective area of approximately 7000 cm^2 and a field of view of $\sim 1^\circ$ full width half half maximum.

Background light curves were generated using the background estimator models based on the rate of very large events (VLE), spacecraft activation and cosmic X-ray emission with the standard PCA analysis tools (ftools) and were subtracted from the source light curve obtained from the event data. The background subtracted light curves were corrected with respect to the barycenter of the solar

Table 3.2: RXTE Pulse Period Measurements of 4U 1907+09

Epoch(MJD)	Pulse Period (sec)	Ref.
45576	437.483 ± 0.004	Makishima et al., 1984
45850	437.649 ± 0.019	Cook & Page 1987
48156.6	439.19 ± 0.02	Mihara 1995
50134	440.341 ± 0.014	in't Zand et al., 1998
50440.4	440.4877±0.0085	This work
51021.9	440.7045±0.0032	This work
51080.9	440.7598±0.0010	This work

Table 3.3: Timing Solution of 4U 1907+09 for RXTE Observations[a] :

Orbital Epoch (MJD)	50134.76(6)[b]
P_{orb} (days)	8.3753(1)[b]
a_x sin i (lt-sec)	83(2)[b]
e	0.28(4)[b]
w	330(7)[b]
Epoch(MJD)	50559.5011(3)
Pulse Period (sec)	440.5738(2)
Pulse Period Derivative (s s^{-1})	6.18(1)× 10^{-9}
Pulse Freq. Derivative (Hz s^{-1})	-3.188(6)×10^{-14}

[a] Confidence intervals are quoted at the 1 σ level.

[b] Orbital parameters are taken from in't Zand et al., 1998 et al., (1997). P_{orb}=orbital period, a_x sin i=projected semimajor axis, e=eccentricity, w=longitude of periastron.

system. Using the binary orbital parameters of 4U 1907+09 from RXTE observations (In 't Zand, Baykal & Strohmayer 1998), the light curves are also corrected for binary motion of 4U 1907+09 (see Table 3.3). From the long archival data string outside the intensity dips, pulse periods for 4U 1907+09 were found by folding the time series on statistically independent trial periods (Leahy et al. 1983). Master pulses were constructed from these observations by folding the data on the period giving the maximum χ^2. The master pulses were arranged in 20 phase bins and represented by their Fourier harmonics (Deeter & Boynton 1985) and cross-correlated with the harmonic representation of average pulse profiles from each observation. The pulse arrival times are obtained from the cross-correlation analysis. We have measured three new pulse periods from the longer observations. These are presented in Figure 3.1 and listed in Table 3.2. We have found that the rate of change of the pulse period of 4U 1907+09 is stable. Therefore we have been able to connect all pulse arrival times in phase over a 383 day time span. The pulse arrival times are fitted to the quadratic polynomial

$$\delta\phi = \phi_o + \delta\nu(t - t_o) + \frac{1}{2}\dot{\nu}(t - t_o)^2 \tag{3.1}$$

where $\delta\phi$ is the pulse phase offset deduced from the pulse timing analysis, t_o is the mid-time of the observation, ϕ_o is the phase offset at t_o, $\delta\nu$ is the deviation from the mean pulse frequency (or additive correction to the pulse frequency), and $\dot{\nu}$ is the pulse frequency derivative of the source. The pulse arrival times (pulse cycles) and the residuals of the fit after the removal of the quadratic polynomial are presented in the Figure 3.2 and Figure 3.3 respectively. Table

3 presents the timing solution of 4U 1907+09. The pulse frequency derivative $\dot{\nu} = (-3.188 \pm 0.006) \times 10^{-14}$ Hz s^{-1} is measured from the pulse arrival times obtained in a sequence of 19 observations spread over 383 days. This value is consistent within 10 % with the long term value obtained from the data displayed in Figure 3.1, $\dot{\nu}$ = (-3.54 $\pm$0.02) $\times 10^{-14}$ Hz s^{-1}. The residuals of the fit give a random walk noise strengths at $T_{observation} \sim$ 383 days, S$\approx (2\pi)^2 < \delta\phi^2 > /T^3_{observation} \approx (2\pi)^2 < \delta\nu^2 > /T_{observation} \sim 2 \times 10^{-20}$ rad^2 sec^{-3}, where $< \delta\phi^2 >$ and $< \delta\nu^2 >$ are the normalized variances of pulse arrival times and residual pulse frequencies (see Cordes 1980 for further definitions of noise strength). This value is 4 decades lower than that of Vela X-1 (Bildsten et al., 1997) and it is only a factor 5 greater than that of the LMXRB pulsar 4U 1626-67 (Chakrabarty et al., 1997). The noise strength of 4U 1626-67 was considered the smallest ever measured for an accretion powered X-ray source. This noise strength is indeed very low for a HMXRB pulsar. The stable spin down rate over the 15 years and the low level of noise strength is a unique property of this source among the HMXRBs. The spin down rate of 4U 1907+09 is only a factor four greater than that of the AXP source 1E 2259+586. Furthermore the long term noise strength is one order of magnitude lower than the AXP 1E 2259+586 (Baykal & Swank 1986). The quiet and persistent spin down rate of 4U 1907+09 shows that an accreting pulsar can spin down quietly, for extended periods. For the AXPs as well as 1E 2259+586, the existence of long epochs of spin down has been interpreted as evidence that these sources are isolated pulsars in dipole spin down in which case the large spin down rates and periods would indicate large

(10^{14}-10^{15} Gauss) magnetic fields (Thompson & Duncan 1993). The existence of known accreting sources with quiet and persistent spin down, as observed from 4U 1626-67, and now 4U 1907+09 shows that quiet spin down does not necessarily imply that the source is not accreting.

CHAPTER 4

2S 1417-62

4.1 Introduction

The X-ray source 2S 1417-62 was detected by SAS-3 in 1978 (Apparao et al. 1980). Analysis of the SAS 3 observations showed evidence of $\sim$ 57 mHz pulsations (Kelley et al. 1981). Einstein and optical observations identified a Be star companion at a distance of 1.4-11.1 kpc (Grindlay et al. 1984). From the timing analysis of BATSE observations between August 26, 1994 and July 7, 1995, orbital parameters were determined and a correlation was found between spin-up rate and pulsed flux (Finger, Wilson & Chakrabarty 1996). Orbital period and eccentricity of the source were found to be 42.12 days and 0.446 respectively.

A "Be star" is an early type non-supergiant star which has a circumstellar disc emanating from its rotational equator which is thought to be formed possibly by fast spin rotation, non-radial pulsations or magnetic loops (Slettebak 1988). Most of the Be/X-ray binary pulsar systems like 2S 1417-62 show recurrent X-ray outbursts that are thought to be mainly due to the fact that the neutron star is accreting material from the Be star's circumstellar disc (Negueruela 1998).

In this chapter, we will present and discuss our timing and spectral analysis of RXTE PCA observations of 2S 1417-62. In Section 2, we will present our

timing and spectral analysis. In Section 3, we will discuss our results, and make conclusions.

4.2 Observations and Data Analysis

We analyzed RXTE archival observations of 2S 1417-62 between November 22,1999 and August 7, 2000 (See Table 4.1 for observation list). The results presented here are based on data collected with the Proportional Counter Array (PCA; Jahoda et al., 1996) and the High Energy X-ray Timing Experiment (HEXTE; Rotschild et al. 1998). The PCA instrument consists of an array of 5 proportional counters (PCU) operating in the 2-60 keV energy range, with a total effective area of approximately 7000 cm^2 and a field of view of $\sim 1^\circ$ FWHM. Although the number of active PCU's varied between 1 and 5 during the observations, observations after 13 May 2000 belongs to the observational epoch for which background level for one of the PCUs (PCU0) increased due to the fact that this PCU started to operate without a propane layer. Newest combined background models (CM) were used together with the latest FTOOLS release (5.2) to estimate the appropriate background. The HEXTE instrument consists of two independent clusters of detectors, each cluster containing four NaI(Tl)/CsI(Na) phoswich scintillation counters (one of the detectors in cluster 2 is not used for spectral information) sharing a common $\sim 1^\circ$ FWHM. The field of view of each cluster was switched on and off source to provide background measurements. The net open area of the seven detectors used for spectroscopy is $1400cm^2$. Each detector covers the energy range 15-250 keV.

Figure 4.1: Background subtracted PCA count rate normalized to 5 PCUs in 3-20 keV band, frequency history before and after orbit subtraction are plotted against time. 5th degree polynomial fit to the orbit subtracted frequency history is overplotted. Initial time value corresponds to November 22, 1999, while the peak of the main outburst is about 50 days later than this date. Note that in some parts of the data, frequencies could not be estimated. These frequency values were left blank. All of the errors are in 1σ level. Vertical dashed lines indicate the orbital phase corresponding to periastron passages.

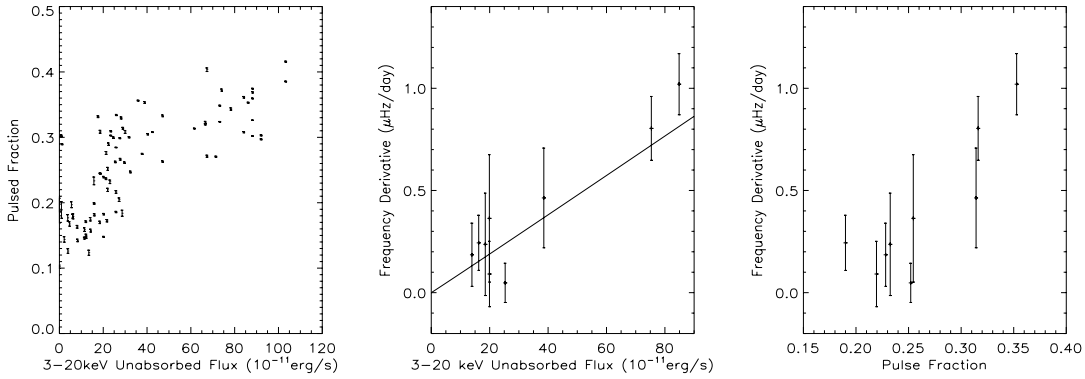

Figure 4.2: **(left)** Pulse fraction versus 3-20 keV unabsorbed X-ray flux. $(F_{max} - F_{min})/(F_{max} + F_{min})$ definition is used to calculate pulse fractions where F_{max} and F_{min} are the highest and lowest fluxes of the phase bins.**(middle)** Pulse Frequency Derivative versus 3-20 keV unabsorbed X-ray flux. Frequency derivatives were found by linear fitting of $\sim$ 20 day intervals of frequency history. X-ray fluxes were found by averaging the corresponding X-ray flux values. Solid line indicates best power law fit with the power index 1.01. **(right)** Pulse frequency derivative versus pulse fraction. Pulse frequency derivatives from the middle panel of this figure were plotted against pulse fractions which were found by averaging corresponding pulse fraction values. Errors in all of the panels are in 1σ level.

Analyzed observations consist of a main outburst that lasted for two orbital periods, followed by a series of mini outbursts each lasting for a single orbit. Duration of the main outburst and the mini outbursts are consistent with those covered in 1994 BATSE observations.

4.2.1 Timing Analysis

Background light curves were generated using the background estimator models based on the rate of very large solar events, spacecraft activation and cosmic X-ray emission with the standard PCA analysis tools and were subtracted from the source light curve obtained from the event data. The background subtracted light curves were corrected to the barycenter of the solar system.

Pulse frequencies for 2S 1417-62 were found by folding the time series on

Table 4.1: Observation List for 2S 1417-62

Time of Observation day/month/year	Exposure ksec	XTE Obs ID
01-29/12/1999	58.7	40051
31/12/1999-19/01/2000	83.2	40070
22-30/11/1999 & 25/01-29/02/2000	125.0	40436
03/03-07/08/2000	127.1	50095

statistically independent trial periods (Leahy et al. 1983). Master pulses were constructed from these observations by folding the data on the period giving the maximum χ^2. The master pulses were arranged in 20 phase bins, represented by their Fourier harmonics (Deeter & Boynton 1985), and cross-correlated with the harmonic representation of average pulse profiles from each observation. The pulse arrival times were obtained from the cross-correlation analysis.The observations of 2S 1417-62 are irregularly spaced, with many gaps of a week or more. In these gaps, pulse frequency derivatives can cause cycle count ambiguity. Therefore, we obtained the pulse frequencies using the pulse arrival times from short segments of the data spans which are typically couple of days. Then the resulting pulse frequencies were orbitally corrected using the binary orbit parameters found from BATSE observations. In fitting of pulse frequencies for the orbit model, we left the orbital epoch as free parameter and used the the orbital parameters given by Finger et al. (1996). We found the new epoch to be JD 2551612.67 ∓ 0.05 and the new orbital period to be 42.19 ∓ 0.01 days, while other orbital parameters were left unchanged. Evolution of PCA count rate, pulse frequency prior to orbital correction, and orbitally corrected pulse frequency were plotted in Figure

Table 4.2: Spectral Parameters of PCA Observations of 2S 1417-62

Time (day)	n_H (10^{22}cm^{-2})	Fe Energy (keV)	Fe Sigma (keV)	Fe Norm. (cts.cm^{-2}.s^{-1})	PL Index	
50.7	4.22 ∓ 0.23	6.75 ∓ 0.12	1.15 ∓ 0.13	$(1.38 \mp 0.41)10^{-3}$	0.90 ∓ 0.02	
101.9	0.24 ∓ 0.24	6.48 ∓ 0.25	0.22 ∓ 0.20	$(4.98 \mp 2.50)10^{-5}$	2.00 ∓ 0.30	
126.7	4.53 ∓ 0.61	6.87 ∓ 0.10	0.96 ∓ 0.28	$(3.18 \mp 1.50)10^{-4}$	1.27 ∓ 0.05	
Time (day)	PL Norm (cts.keV$^{-1}\times$ cm^{-2}.s^{-1})	E_{cut} (keV)	E_{fold} (keV)	Reduced χ^2	3-20 keV Flux (absorbed) (ergs.cm^{-2}.s^{-1})	3-20 keV Flux (unabsorbed) (ergs.cm^{-2}.s^{-1})
50.7	$(3.31 \mp 0.15)10^{-2}$	11.02 ∓ 0.13	22.71 ∓ 0.63	1.56	9.79×10^{-10}	1.05×10^{-9}
101.9	$(3.72 \mp 1.12)10^{-3}$	18.03 ∓ 5.00	30.40 ∓ 6.00	0.68	1.17×10^{-11}	1.17×10^{-11}
126.7	$(1.57 \mp 0.18)10^{-2}$	10.97 ∓ 0.72	22.27 ∓ 1.95	1.05	1.98×10^{-10}	2.12×10^{-10}

4.1.

Individual pulse profiles were used to calculate pulse fractions. Relation between pulse fraction and 3-20 keV unabsorbed X-ray flux was plotted in the left panel of Figure 4.2. 8 pulse profiles corresponding to different flux levels were plotted in Figure 3. Spin-up rates were found by linear fitting of the $\sim$ 20 day long segments of frequency time series. In these time intervals, 3-20 keV unabsorbed X-ray flux and pulse fraction values were recalculated by averaging corresponding unabsorbed X-ray flux and pulse fraction values. Relations among frequency derivative, recalculated pulse fraction and recalculated 3-20 keV unabsorbed X-ray flux were plotted in middle and right panels of Figure 4.2.

4.2.2 Spectral Analysis

Spectrum,background and response matrix files were created using *FTOOLS* 5.2 data analysis software. Background spectra were generated using the background estimator models based on the rate of very large solar events, spacecraft activation and cosmic X-ray emission.

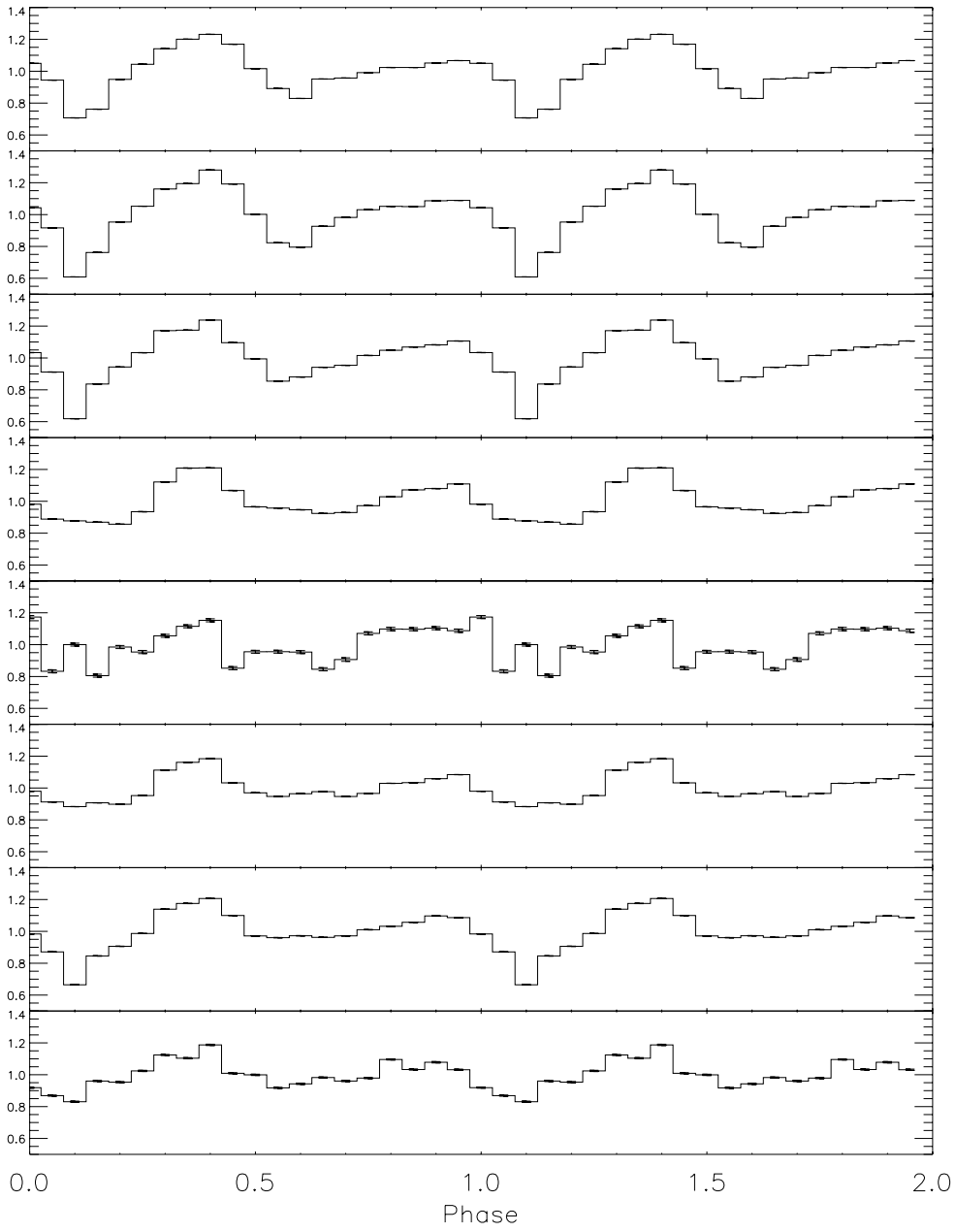

Figure 4.3: **(top to bottom)** Pulse profiles for days ~ 31.2 (rise of the mainoutburst), ~ 50.6 (peak of the main outburst), ~ 76.2 (peak of the main outburst at the second orbit), ~ 95.3 (decline of the main outburst), ~ 101.9 (low X-ray flux part), ~ 107.1 (rise of the mini outburst), ~ 124.1 (peak of the mini outburst), and ~ 137.4 (decline of the mini outburst). Corresponding 3-20 keV unabsorbed fluxes in units 10^{-11}ergs.cm^2.s^{-1} are 75.1, 105.1, 54.0, 11.9, 1.18, 11.9, 21.9, and 3.69 respectively. Phases of the pulse profiles were manually aligned by using the similarities in the pulse shapes

.

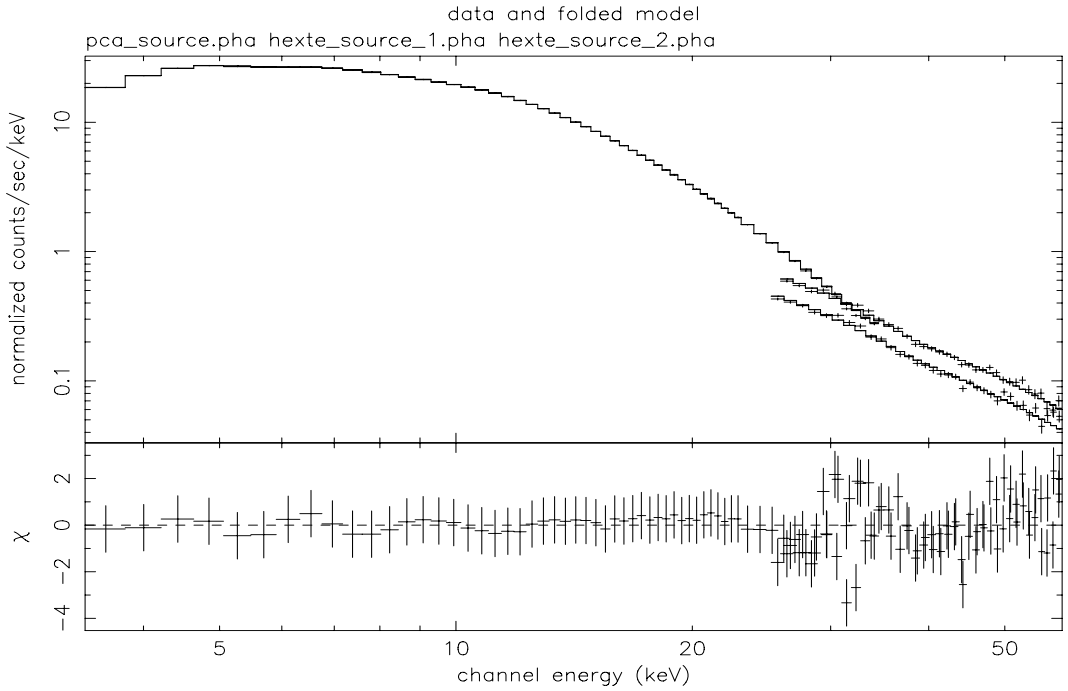

Figure 4.4: Combined PCA and HEXTE spectrum for the dataset 40070. The bottom panel shows the residuals of the fit in terms of σ values.

Spectral analysis and error estimation of the spectral parameters were performed using *XSPEC* version 11.1. Overall PCA (3-35 keV) and HEXTE (25-60 keV) spectra were constructed for the main outburst covered by the dataset 40070 (Figure 4). Individual PCA spectra were constructed for the same time intervals that were used for calculating arrival times. Energy channels corresponding to 3-20 keV energy range were used to fit the spectra. Energies lower than 3 keV were ignored due to uncertainties in background modeling while energies higher than 20 keV were ignored as a result of poor counting statistics. No systematic error was added to the errors.

Appropriate spectral model for both overall 3-55 keV (PCA-HEXTE) spectrum and individual 3-20 keV band (PCA) spectra was found to be a power law model with low energy absorption (Morrison & McCammon, 1983), multiplied by an exponential high energy cut-off function (White et al. 1983). Additional Iron emission line complex modeled as a Gaussian at $\sim 6.4 - 6.8$ keV was required as the part of the spectral model. Evolution of spectral parameters of 3-20 keV PCA spectrum was plotted in Figure 4.2.2. Spectral parameters corresponding to the overall PCA-HEXTE spectra and these 3 regions were listed in Table 4.2 and 4.3 respectively. Using individual 3-20 keV spectra, hydrogen column density was found to be correlated with the 3-20 keV X-ray flux, while power law index was found to be anti-correlated with the 3-20 keV X-ray flux (see Figure 4.5).

Using XSPEC software and assuming a distance of 11 kpc, 3-20 keV band luminosities were found to be $\simeq 1.4 \times 10^{34}$ ergs/s for the low X-ray flux regions between outbursts, $\simeq 1.3 \times 10^{36}$ ergs/s for the peak of the main outburst, and

Table 4.3: Spectral Parameters of PCA-HEXTE Observations of the main outburst of 2S 1417-62

Parameter	Value
Hydrogen Column Density (10^{22}cm^{-2})	3.99 ∓ 0.14
Gaussian Line Energy (keV)	6.82 ∓ 0.16
Gaussian Line Sigma (keV)	1.08 ∓ 0.15
Gaussian Normalization (cts.cm^{-2}.s^{-1})	$(1.20 \mp 0.15) \times 10^{-3}$
Power Law Photon Index	0.90 ∓ 0.02
Cut-off Energy (keV)	11.1 ∓ 0.6
E-folding Energy (keV)	21.6 ∓ 1.3
Power Law Normalizations (cts.keV^{-1}.cm^{-2}.s^{-1})	$(2.77 \mp 0.23) \times 10^{-2}$
Calculated X-ray Fluxes (3-60 keV in ergs.cm^{-2}.s^{-1})	
— Absorbed	1.59×10^{-9}
— Unabsorbed	1.65×10^{-9}
Reduced χ^2	1.01 (119 d.o.f)

$\simeq 2.3 \times 10^{35}$ ergs/s for the peak of the first mini outburst followed by the main outburst.

4.3 Discussion and Conclusion

In a Be/neutron star binary system, occasional X-ray outbursts may be observed, implying the neutron star is accreting material, presumably from the Be star's circumstellar disc if the circumstellar disc undergoes a sufficiently large increase in its radial extent and density to intersect the neutron stars orbital path. The neutron star may stop accreting and ceases to be apparent as a bright X-ray source after the Be circumstellar disc has contracted.

The pattern of X-ray outbursts is affected by the size, eccentricity and orientation of the neutron star's orbit with respect to the Be star. The orbit could be coplanar with the Be circumstellar disc or offset such that the neutron star may pass through the circumstellar disc. In the latter case, neutron star may either

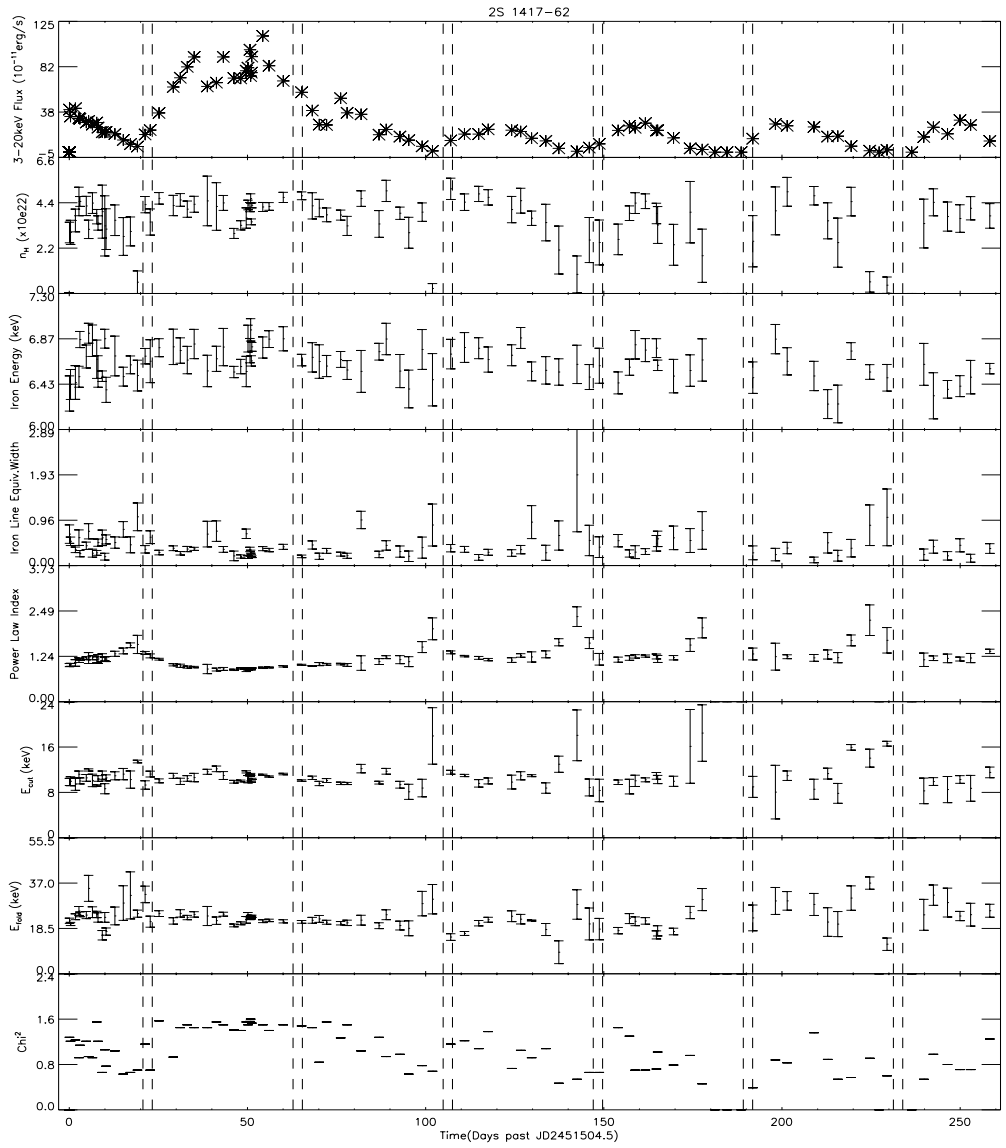

Figure 4.5: Evolution of Hydrogen column density, Iron line complex peak energy, iron line equivalent width, power law index, power law normalization, cut-off energy, folding energy, and reduced χ^2. Vertical dashed lines indicate the orbital phase corresponding to periastron passages.

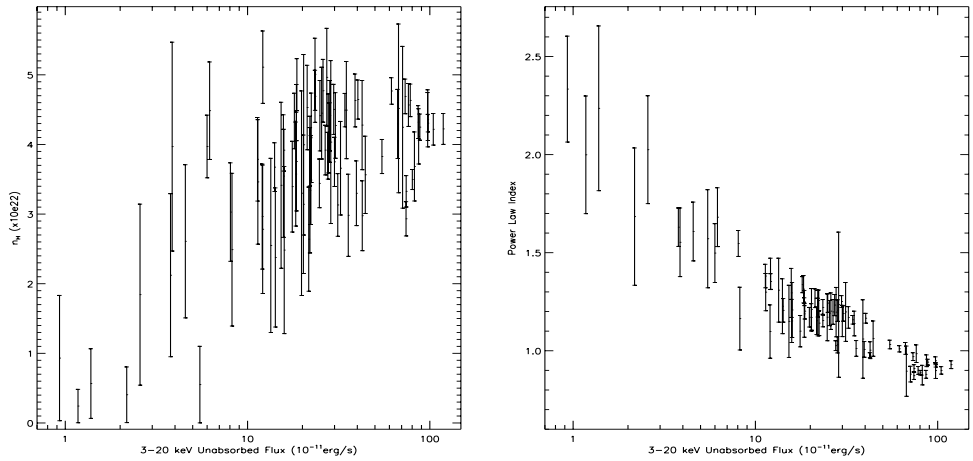

Figure 4.6: **(left)** Hydrogen column density as a function of 3-20 keV unabsorbed X-ray flux. **(right)** Power law index as a function of 3-20 keV unabsorbed X-ray flux.

pass through the disc twice per orbit or pass only once per orbit as in the case for 2S 1417-62.

There are basically two accretion modes possible for the neutron star in a Be/Neutron star binary system. The first possible mode is direct accretion of the Be circumstellar disc material by the neutron star during the circumstellar disc passage in a manner similar to a wind-fed pulsar experiencing Bondi-Hoyle type accretion. For this mode of accretion, there will be less efficient angular momentum transfer compared to a standard disc accretion. This mode accretion may be considered to be the cases for the X-ray spikes during the periastron and for the mini outbursts of 2S 1845-024 respectively (Finger et al. 1999).

The second mode that actually seems to be the case for 2S 1417-62 is accretion after the bound material has collapsed into a standard but temporary (lasting for about one single orbital period for mini outbursts, and about two orbital

periods for the main outburst) accretion disc. In case the accretion is from a Keplerian disc that has formed due to the passage of the neutron star from the equatorial disc of the companion, the magnetosphere of the neutron star disturbs the Keplerian rotation of the disc at the inner disc edge, forcing matter to flow along magnetic field lines to the vicinity of the magnetic poles. An accretion disc can transfer angular momentum either at the vicinity of the magnetospheric radius where the disc began to be disrupted and the material is channeled from the inner edge of the disc to the magnetic poles, or from the overall interaction of the accretion disc and magnetic field lines of the neutron star (i.e threading of the field lines into the accretion disc without disrupting the disc). Thus, the total accretion torque is the resultant of the torques produced by the angular momentum of the matter that falls onto the neutron star (material torque) and the torque produced by the interaction of the magnetic field lines and the accretion disc (magnetic torque). Material torque from a prograde accretion disc, being proportional to mass accretion rate, always acts to spin-up the neutron star, while magnetic torque can either be negative or positive. The contribution of torque from the magnetic field lines threading the disc outside the corotation radius r_{co} is negative. Therefore, resultant torque can either be a spin-up (positive) or a spin-down (negative) torque.

Assuming observed X-ray luminosity is proportional to the bolometric luminosity (or mass accretion rate), spin-up rate and X-ray flux correlation can be explained by accretion from accretion disks when the net torque is positive and of the order of the material torque (Ghosh & Lamb 1979; Ghosh 1993). Correlation

between spin-up rate and X-ray flux in different X-ray energy bands has been observed in outbursts of other transient X-ray pulsar systems: EXO 2030+375 (Wilson et al. 2002; Parmar, White & Stella 1989), A 0535+26 (Bildsten et al. 1997; Finger, Wilson & Harmon 1996), 2S 1845-024 (Finger et al. 1999), GRO J1744-28 (Bildsten et al. 1997), GRO J1750-27 (Scott et al. 1997), XTE J1543-568 (In't Zand, Corbet & Marshall 2001), and SAX J2103.5+4545 (Baykal, Stark & Swank 2002). Correlation between 20-50 keV X-ray flux and spin-up rate was previously found for 2S 1417-62 using BATSE observations (Finger, Wilson & Chakrabarty 1996). Our analysis of RXTE datasets of 2S 1417-62 has also showed the evidence of this correlation for both the main outburst and the following mini outbursts in 3-20 keV band (see the middle panel of Figure 4.2).

When the neutron star in a Be/neutron star binary system leaves the dense equatorial disc of the companion, the accretion disc can no longer be fed by the surrounding material. In this case, accretion disc may disappear. When there is no accretion disc, the neutron star may either continue to accrete from the non-equatorial wind of the companion or may enter propeller phase (Illarionov & Sunyaev 1975). In case accretion is the result of the companion's non-equatorial wind when the neutron star is away from the equatorial disc of the companion star, it is possible to see erratic spin-up and spin-down episodes (just like wind accreting systems, see Bildsten et al. 1997; Inam & Baykal 2000) which is not the case in 2S 1417-62 even for the lowest flux parts of our datasets. However, in case of any change in accretion regime including transition from disc to wind accretion, we expect changes in the morphology of the pulse profiles. In case

wind of the companion does not cause accretion, propeller phase may set in. In the propeller phase, we may expect spin pulsations to cease accompanied by a decrease in flux (Cui 1997), although it may also be the case that the pulsations do not cease completely even in the propeller phase (Neguerela et al. 2000).

Although we did not observe any erratic spin-up and spin-down episodes in the archival data, we found that both pulse fraction and shape of pulse profiles have dependence on the X-ray flux (Figures 2 and 3). From Figure 3, we found that the morphology of pulse profiles for the peaks of the main outburst and the mini outbursts as well as the increasing flux regions just after the periastron and declining flux regions before the next periastron passages are similar, with only a slight difference in the pulse fractions. However, both the pulse fraction and the morphology of the pulse profiles of the low flux parts of the data is considerably different from the data elsewhere. Similarity of the pulse profiles of the main outburst and the mini outbursts may indicate that we basically have the same accretion geometry with slightly different mass accretion rate. Together with the fact that the spin up rate is correlated with the flux, we may argue that we have disc accretion for all stages of the main outburst and mini outbursts with a varying mass accretion rate but basically with the same accretion geometry. Decreasing pulse fraction accompanied with changing pulse morphology for the low flux parts may indicate changes in accretion geometry and even be an indicator of a transition from disc to wind accretion, or an ongoing transition from accretor phase to propeller phase. SAX J2103.5+4545 is a counter-example for which no significant changes in pulse fraction and pulse profiles are seen with

changing flux (Baykal, Stark & Swank 2002). Therefore, accretion geometry and polar cap size of SAX J2103.5+4545 should not be related considerably to the mass accretion rate while 2S 1417-62 may have such accretion geometry changes accompanied with the decrease in X-ray flux. Correlation between spin-up rate and pulse fraction is also another evidence of such a transition (see right panel of Figure 4.2).

Decline of the X-ray flux may be an indication of an ongoing transition from accretor to propeller stage. When the propeller stage sets in, the great majority of accreting matter cannot reach the neutron star and factor of decrease in the bolometric luminosity becomes

$$\Delta = 170 M_{1.4}^{1/3} R_6^{-1} P_0^{2/3}$$

where $M_{1.4}$ is the mass of the neutron star in units of $1.4 M_\odot$, R_6 is the radius of the neutron star in units of 10^6 cm and P_0 is the spin period of the neutron star in units of second (Corbet 1996; Campana & Stella 2000; Campana et al. 2002). Decrease factor Δ becomes $\sim 10^3$ for a neutron star with mass $\sim 1.4 M_\odot$, radius $\sim 10^6$ cm and spin period of ~ 17.5 s . We do not observe such sharp X-ray flux declines in RXTE-PCA observations of 2S 1417-62, moreover a factor of $\sim 10^3$ decrease in X-ray flux of 2S 1417-62 should be considerably less than the background level. As a comparison, 3-20 keV X-ray flux of 2S 1417-62 is lower in the low X-ray flux regions between outbursts by a factor of ~ 15 with respect to peak of mini outbursts and ~ 90 with respect to the peak of the main outburst. These factors seem to be considerably smaller than the expected

factors for accretor to propeller transition. It is more likely that we just observe an accretion geometry change due to decreasing $\dot{M}$, maybe an ongoing transition to propeller, but not the propeller stage itself.

Since 2S 1417-62 is not likely to make transitions to propeller phase, we observe accretion regime of the source even at the lowest flux level. In case of accretion, the minimum luminosities that we have should be greater than a limiting accretion luminosity (L_{limit}) given as: (Stella et al. 1986, Illarionov, Sunyaev 1975)

$$L_{min} > L_{limit} \cong 2 \times 10^{37} R_6^{-1} M_{1.4}^{-2/3} P_0^{-7/3} (\frac{\mu}{10^{30}\mathrm{Gcm}^3})^2 \mathrm{ergs.s}^{-1}$$

where μ ($\cong BR^3$, B being the surface magnetic field of the neutron star) is the magnetic moment of the neutron star. Using the spectral model for low flux part of the data and assuming a distance of 11 kpc -which is within the range of possible distances given by Grindlay et al. (1984)-, 0.5-30 keV X-ray luminosity is found to be $\sim 2.1 \times 10^{34}$ ergs/s. Using this luminosity, and assuming that $R \sim 10^6$cm, $M \sim 1.4 M_\odot$, a lower limit to the magnetic field can be set to be $\sim 9 \times 10^{11}$G, which is consistent with the typical magnetic fields of accretion powered pulsars.

From Figure 4.1, it is evident that the location of the periastron passage is just after the start of both the main outburst and the mini outbursts. The mini outbursts last for almost an entire orbit of 2S 1417-62 and hence indicate the binding of some Be circumstellar disc material to the neutron star during disc passage with the accretion of the bound material occurring during the course of the orbit. The BATSE observations showed a very similar normal outburst

pattern with the hard X-rays (above 20 keV) starting just after periastron passage and ending before the next periastron passage. Pattern and duration of the main outburst is also consistent with the main outburst observed by BATSE, starting just after the periastron and lasting about two orbital periods. Duration of the main outburst indicate that the equatorial disc of the companion is dense enough to provide enough disc material initially to feed the disc for two orbital periods. An increase in X-ray flux during the main outburst is observed corresponding to the periastron passage as well, showing that the neutron star has entered the equatorial disc again, but, this time, without complete depletion of the accretion disc material around it.

Galactic coordinates (l=313.02 b=-1.598) of 2S 1417-62 reveals that the source is almost at the boundary of the galactic ridge region (corresponding to R1 region defined by Valinia, Marshall 1998). Spectral model for the galactic ridge emission includes an absorbed power law model with power law index ~ 1.8 and Raymond Smith component at ~ 3 keV. If the flux of the galactic ridge were comparable to the X-ray flux in the low X-ray flux regions, then we would not be sure about the reality of the higher power law indices and decreasing pulse fractions, since these effects may be due to the fact that our background is contaminated by the galactic ridge emission. However, X-ray flux in 3-20 keV is found to be only $\sim 2.5\%$ of the typical flux for the low X-ray flux region of 2S 1417-62 by using the spectral model for R1 region of the galactic ridge. Therefore, it is not likely that our results are very much affected by the galactic ridge emission.

Spectrum of 2S 1417-62 is found to be consistent with a typical accretion

powered pulsar spectral model consisting of an absorbed power law with power law index $\sim 0.9-1.2$ and an high energy cut-off at $\sim 9-12$ keV. For the low X-ray flux regions between outbursts, power law index is found to be higher reaching values of ~ 2, while cut-off energy increases to $\sim 15-18$ keV but the uncertainty in the cut-off energy increases from ~ 0.5 keV to ~ 5 keV meanwhile.

Although Hydrogen column density is, in general, found to be correlated with the X-ray flux (left panel of Figure 6, it is found to be considerably lower for the low X-ray flux regions between the outbursts where it decreases to $\lesssim 1 \times 10^{22}$ cm^{-2}. Lower hydrogen column densities together with lower X-ray flux at low X-ray flux regions may indicate lower matter concentration around the neutron star due to the fact that neutron star is in the orbital phase away from the equatorial Be wind so that matter around the neutron star has ceased or is about to cease. This is also related to the fact that the X-ray flux decreases, since $\dot{M}$ of the accretion disc decreases due to the lower density of the surrounding material feeding the disc..

Iron line complex at $\sim 6.4-6.8$ keV is found to exist for the overall data. This energy range shows that the iron line complex is composed not only of cold fluorescent Iron K line at ~ 6.4 keV, but also of H-like and He-like Iron lines $\sim 6.7-7.0$ keV which is possibly emitted from hot and ionized gas around neutron star, e.g. accretion disc corona. We are unable to resolve this line complex into single emission lines in each RXTE observation. Although uncertainty in iron line energy is almost comparable to the changes in the iron line energy, there is still a weak trend that the peak energy of the iron line is found to be $\sim 6.4-6.5$

keV at or near low X-ray flux parts of the data, while the peak energy reaches sim $\sim 6.7 - 6.8$ keV near the X-ray flux maxima of the outbursts. A plausible explanation for this trend of the peak energy is that density of the ionized gas around the neutron star increases while outbursts occur. Future observations with new X-ray observatories like XMM-Newton and Chandra may be useful to resolve this iron line complex features in 2S 1417-62.

Anti-correlation of power law index with the X-ray flux is an indication of the fact that spectrum gets softened with decreasing X-ray flux. (right panel of Figure 4.2.2). Spectral hardening is observed in the low state spectra of neutron star soft X-ray transients like Aql X-1, which may be interpreted to be a sign of propeller stage (Zhang et al. 1998) or a sign of a turned-on rotation powered pulsar (Campana et al. 1998). On the other hand, increasing power law indices (i.e softening of the spectra) with decreasing flux might be the consequence of mass accretion rate changes only (see e.g models for low luminosity X-ray sources by Meszaros et al. 1983; Harding et al. 1984). In this case, neither a transition to propeller stage nor an accretion geometry change is needed to explain the softening in the spectrum accompanied by decreasing flux. Consequently, decrease in mass accretion rate, accompanied by a softening in the spectrum, does not lead to any significant changes in pulse profiles and pulse fraction (e.g. Baykal, Stark & Swank 2002 for SAX J2103.5+4545). We have a similar situation in 2S 1417-62 except that in the lowest X-ray flux parts, spectral softening of 2S 1417-62 is accompanied by the changes in pulse profiles and pulse fractions. Therefore, spectral softening observed throughout main outburst and mini outbursts may

be similar to the case in the case in SAX J2103.5+4545, however spectral softening in 2S 1417-62 may be the result of not only accretion rate changes but also accretion geometry changes for the low flux parts, which occur just before the periastron for which the neutron star should have accreted almost all of the accretion disc material around it.

New X-ray observations which will monitor main high outbursts, the following mini outbursts and X-ray dips continuously so that the data will be continuously phase-connected will be very useful for further studies of 2S 1417-62. These observations will help us to understand the accretion mechanism better and test the possible transition from accretor to propeller stage. New observations may also be useful to revise and improve orbital parameters and to have a better understanding of timing and spectral evolution of 2S 1417-62.

CHAPTER 5

SAX J2103.5+4545

5.1 Introduction

The transient X-ray source SAX J2103.5+4545 was discovered by the Wide Field Camera on the *BeppoSAX* X-ray observatory during its outburst between 1997 February and September with 358.61s pulsations and a spectrum consistent with an absorbed power law model with the photon index of ~ 1.27 and the absorption column density of $\sim 3.1 \times 10^{22}\mathrm{cm}^{-2}$ (Hulleman, in't Zand, & Heise 1998).

After detection of another outburst in November 1999 by the *all-sky monitor (ASM)* on the *Rossi X-ray Timing Explorer (RXTE)*, the source was found to be active for more than a year, and was continuously monitored through regular pointed *RXTE* observations. Using pulse arrival times, the orbital period and eccentricity of the orbit were found to be 12.68(25) days and 0.4(2) (Baykal, Stark, & Swank 2000a,b). In the timing analysis, the source was initially found to be spinning up for ~ 150 days, at which point the flux dropped quickly by a factor of $\simeq 7$, and a weak spin-down began afterwards (Baykal, Stark, & Swank 2002). Strong correlation between X-ray flux and spin-up rate was explained by using Ghosh & Lamb (1979) accretion disk model. The X-ray spectra well fitted

the absorbed power law model with high energy cutoff and a ∼6.4 keV fluorescent emission line (Baykal et al. 2002).

Orbital parameters found by using *RXTE* observations of the source (Baykal et al. 2000a,2000b) indicated that the source has a high mass companion. Hullemann et al. (1998) pointed out a B8 type star within the BeppoSAX error box, but its distance ($\sim$ 0.7 kpc) implied a luminosity too low to explain the spin-up that was seen in the RXTE observations. Recently, a possible candidate for the optical companion of SAX J2103.5+4545 with the visual magnitude of 14.2 was discovered (Reig & Mavromatakis, 2003).

SAX J2103.5+4545 was also observed with the *INTEGRAL* observatory in the 3-200 keV band with significant detection up to $\sim$ 100 keV (Lutovinov, Molkov,& Revnivtsev 2003). The spectral parameters found in the *INTEGRAL* observations of the source were found to be compatible with those found by Baykal et al. (2002).

Since the beginning of the most recent outburst in June 2002, SAX J2103.5+4545 has been monitored continuously by *RXTE* through regular pointed observations. It was possible to obtain some simultaneous coverage with the *XMM-Newton* observatory on January 6, 2003. The observation of *XMM-Newton* revealed a soft spectral component of the source which was well-represented by a blackbody model. This spectral model was verified by simultaneous fitting of January 6, 2003 *RXTE*-PCA observation. Using *XMM-Newton* dataset, we also discovered $\sim$ 22.7s quasi periodic oscillations (QPO's) of this source for the first time. In this paper, we present our spectral and timing results of the analysis of RXTE

and XMM datasets of SAX J2103.5+4545.

5.2 Observations

5.2.1 RXTE

We analyzed RXTE observations of SAX J2103.5+4545 between December 3, 2002 and January 29, 2003 with a total observation time of $\sim$ 52ksec. This set of observations is a subset of the RXTE observations for the proposal number 70082. The results presented here are based on data collected with the Proportional Counter Array (PCA; Jahoda et al., 1996). The PCA instrument consists of an array of 5 proportional counters (PCU) operating in the 2-60 keV energy range, with a total effective area of approximately 6250 cm^2 and a field of view of $\sim 1^\circ$ FWHM. Although the number of active PCU's varied between 2 and 5 during the observations, our observations belong to the observational epoch for which background level for one of the PCUs (PCU0) increased due to the fact that this PCU started to operate without a propane layer. The latest combined background models (CM) were used together with FTOOLS 5.2 to estimate the appropriate background.

5.2.2 XMM

XMM-Newton observations took place on January 6, 2003 with an 8.7 ksec continuous exposure. Among the three EPIC detectors (Turner et al. 2001; Strüder et al. 2001), the MOS1 and MOS2 detectors were configured in Fast

Uncompressed mode, while the PN was configured in Fast Timing mode. Data collected by the EPIC detectors on *XMM-Newton* were processed using version 5.4.1 of the *XMM-Newton* Science Analysis System (SAS). We did not include the data collected by the two Reflection Grating Spectrometers (RGS1 and RGS2) in data analysis since the count rates from these spectrometers were too low.

5.3 Data Analysis

5.3.1 Pulse Timing and Pulse profiles

In the timing analysis, we corrected the background subtracted lightcurves of RXTE data to the barycenter of solar system. The data have also been corrected for the orbit model using the eccentric orbital parameters given by Baykal et al. (2000b) with the new orbital epoch being MJD 52633.90 ∓ 0.05. In order to estimate the pulse frequency and pulse frequency derivative accurately, we used ~ 57.5 days time span of RXTE observations between MJD 52611.48 and MJD 52668.90 which covers ~ 8.7 ksec short observation of XMM data starting at MJD 52645.85. We obtained the nominal pulse frequency by using Fourier transform and constructed 20 pulse profiles (one pulse profile for each RXTE orbit) by folding the lightcurve at this nominal pulse period. We found the pulse arrival times (phase offsets) by cross-correlating these pulse profiles with a template chosen as the most statistically significant pulse profile. In the pulse timing analysis, we used the harmonic representation of the pulse profiles (Deeter & Boynton 1985). In this technique, the pulse profiles are expressed in terms of

harmonic series and cross correlated with the template pulse profile. The pulse phase offsets can be found of a Taylor expansion,

$$\delta\phi = \delta\phi_0 + \delta\nu(t - t_0) + \frac{1}{2}\dot{\nu}(t - t_0)^2, \tag{5.1}$$

where $\delta\phi$ is the pulse phase offset deduced from the pulse timing analysis, t_0 is the midtime of the observation, ϕ_0 is the phase offset at t_0, $\delta\nu$ is the deviation from the mean pulse frequency (or additive correction to the pulse frequency), and $\dot{\nu}$ is the pulsar's pulse frequency derivative. We fitted the phase offsets to the Taylor expansion. From the fit, we found the pulse period corresponding to the XMM observation as 354.7940 ± 0.0008s and 57.5 days average spin-up rate as $(7.4 \pm 0.9) \times 10^{-13}$ Hz s^{-1}. We did not see any significant timing noise in the residuals of arrival times, which indicated that the spin up rate was stable through the observations. The average 3-20 keV flux of RXTE observations was $(5.5 \mp 0.5) \times 10^{-10}$ergs^{-1}cm^{-2}. The mean spin-up rate and the average X-ray flux were found to be consistent with the previously observed spin-up rate and X-ray flux correlations during the 1999 outburst (see Fig. 7 in Baykal et al. 2002). Detailed timing noise of RXTE observations is in progress and is not the scope of this paper (Baykal et al. 2004).

In Figure 5.1, we presented energy dependent pulse profiles of XMM-EPIC PN data. The feature peaking at the phase ~ 0.25 before the peak of the main pulse was a prominent feature of the pulse profile. The pulse fraction was $(50.9 \mp 0.3)\%$ at 0.9-11 keV, whereas it was found to be slightly variable in the energy intervals shown in Figure 5.1 with a minimum of $(48.5 \mp 0.8)\%$ at 7.5-11 keV and

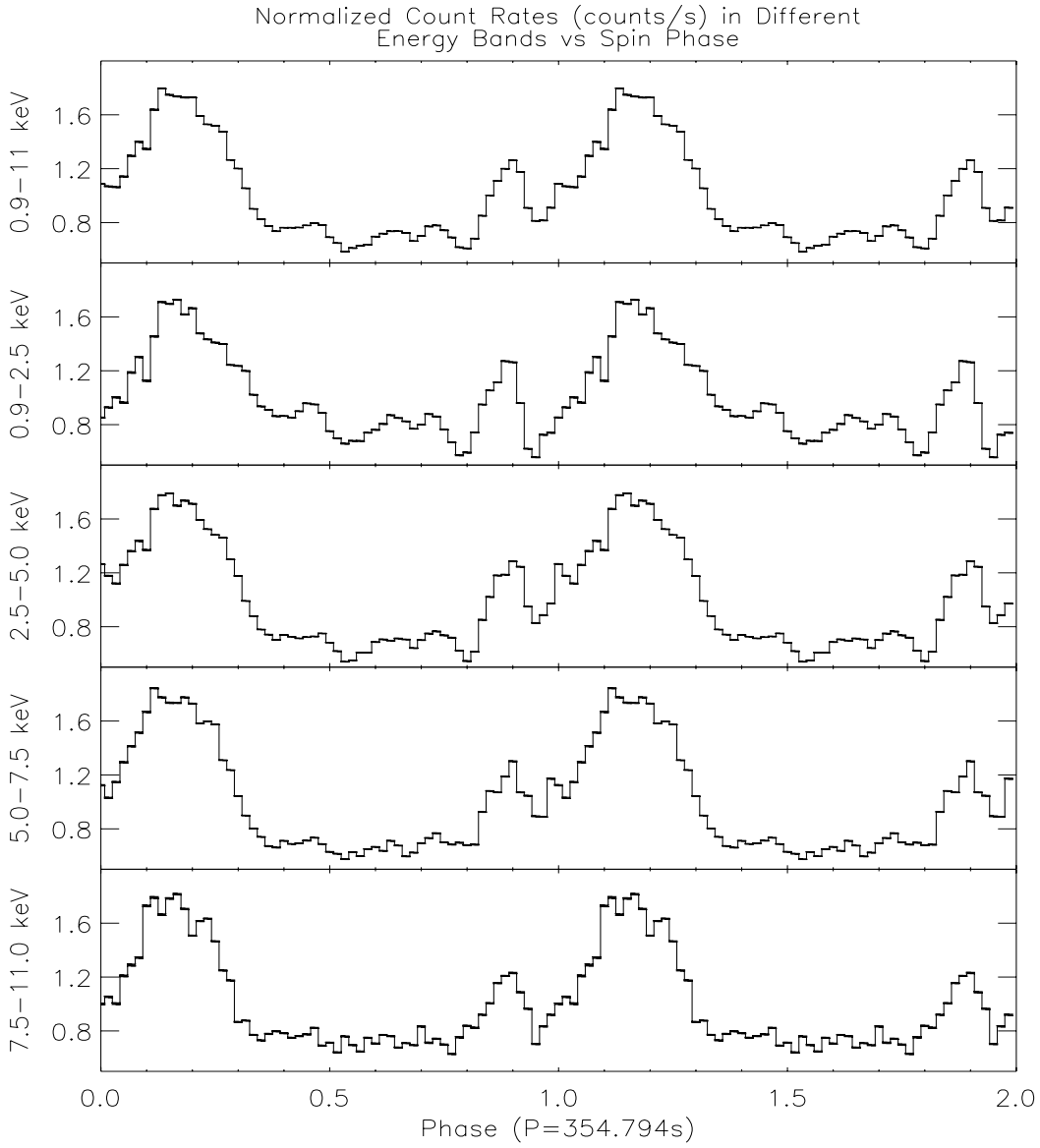

Figure 5.1: Energy dependence of the pulse profiles of SAX J2103.5+4545. Pulse profiles were found by using EPIC-PN lightcurves that cover the energy ranges from top to bottom respectively.

a maximum of $(53.6 \mp 0.7)\%$ at 2.5-5.0 keV.

5.3.2 Transient 22.7 sec QPO

In the power spectra of the 0.9-11 keV EPIC-PN lightcurve we found quasi periodic oscillations around 0.044 Hz (see Figure 5.2). In order to test the significance of these oscillations, we averaged 9 power spectra and rebinned the frequencies by a factor 8. Then we modeled the continuum power spectrum with a broken power law model with the break value $(4.45 \mp 0.16) \times 10^{-2}$ Hz, and the power indices -0.34 ∓ 0.08 and -2.14 ∓ 0.05. We modeled the transient oscillations with a Lorentzian centered at $(4.40 \mp 0.12) \times 10^{-2}$ Hz, with the full width half maximum (FWHM) of $(6.1 \mp 2.0) \times 10^{-3}$ Hz.

To test the significance of this QPO feature, we normalized the power spectrum by dividing it by the continuum and we multiplied this result by 2 (van der Klis 1989). The resultant power spectrum would be consistent with a Poisson distribution for a degree of freedom $2 \times 8 \times 9 = 144$. As seen from the lower panel of Figure 5.2, there is a prominent peak at ~ 0.044 Hz with a minimum of excess power (including the error of power) 3.62 giving the total power as $3.62 \times 8 \times 9 = 260.64$. This gives the probability of detecting a false signal $Q(260.64|144) = 9.39 \times 10^{-9}$. Since we have 512 frequencies in each power spectra, total probability of having false signal becomes $9 \times 512 \times 9.39 \times 10^{-9} = 4.3 \times 10^{-5}$. Therefore significance of transient oscillations is $1 - 4.3 \times 10^{-5} \simeq 0.99996$ which is consistent with more than 6 sigma level detection. The rms fractional amplitude associated with this QPO feature was found to be $(6.6 \mp 1.9)\%$.

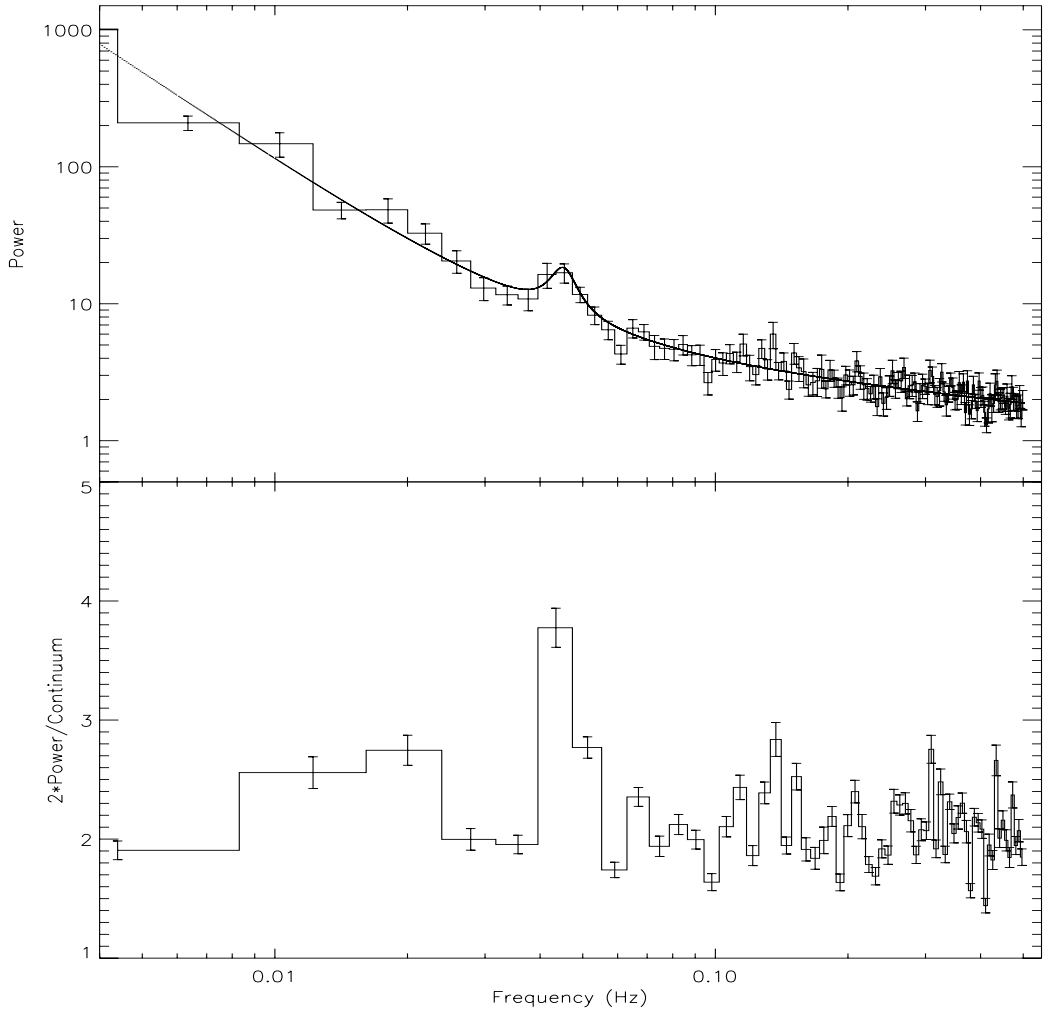

Figure 5.2: **(top)** Power spectrum obtained from the 0.9-11.0 keV EPIC-PN lightcurve and rebinned by a factor of 4. QPO feature centered at 0.044 Hz is the prominent feature of the power spectrum. **(bottom)** Power spectrum rebinned by a factor of 8, multiplied by 2, and divided by the continuum fit consisting of a broken power law model with the power indices -0.34 ∓ 0.08 and -2.14 ∓ 0.05. Applying the method discussed by van der Klis (1989), significance of the QPO feature was calculated to be more than 6σ confidence level using the value of the peak at ~ 0.044 Hz as shown in this plot.

We searched transient oscillations using the RXTE-PCA lightcurves in the 3-20 keV energy range, however we did not see any significant transient oscillations. Then we extracted a $\sim 50\%$ portion of the overall XMM-EPIC PN lightcurve at the 3-10 keV energy range that coincided exactly with the $\sim$ 4.5 ksec part of the RXTE PCA lightcurve on January 6, 2003 and performed power spectral analysis. We found that the significances of 0.044 Hz oscillations for RXTE and XMM lightcurves are 2.5σ and 2.8σ respectively. We concluded that the QPO feature was originated mostly from the soft component of the spectrum or highly transient. Future observations are required to confirm these oscillations.

5.3.3 Spectral Analysis

We fitted overall background subtracted 1-10 keV spectra of PN, MOS1 and MOS2 to an absorbed power law model (Morrison & McCammon, 1983) with high energy cut-off (White, Swank, Holt 1983). In addition, an iron line feature at 6.42 keV was required in the spectral model (Case 1 in Table 5.1). However, this model did not fit the spectrum of the source well, giving a reduced χ^2 of 2.69. Adding an additional blackbody component to the model decreased the reduced χ^2 to 1.23 (Case 2 in Table 5.1). Joint fit including the PCA data on January 6, 2003 and adding 2% systematic errors (see Wilms et al. 1999; Coburn et al. 2000), was possible to this model with a reduced χ^2 of 1.1 (Case 3 in Table 5.1 and Figure 5.3). Using Case 3 (i.e. the joint fit to the model including blackbody component), 1-20 keV unabsorbed flux was found to be 6.6×10^{-10} ergs s^{-1} cm^{-2}. Assuming a source distance of 3.2 kpc (Baykal et al. 2002), this value corresponds

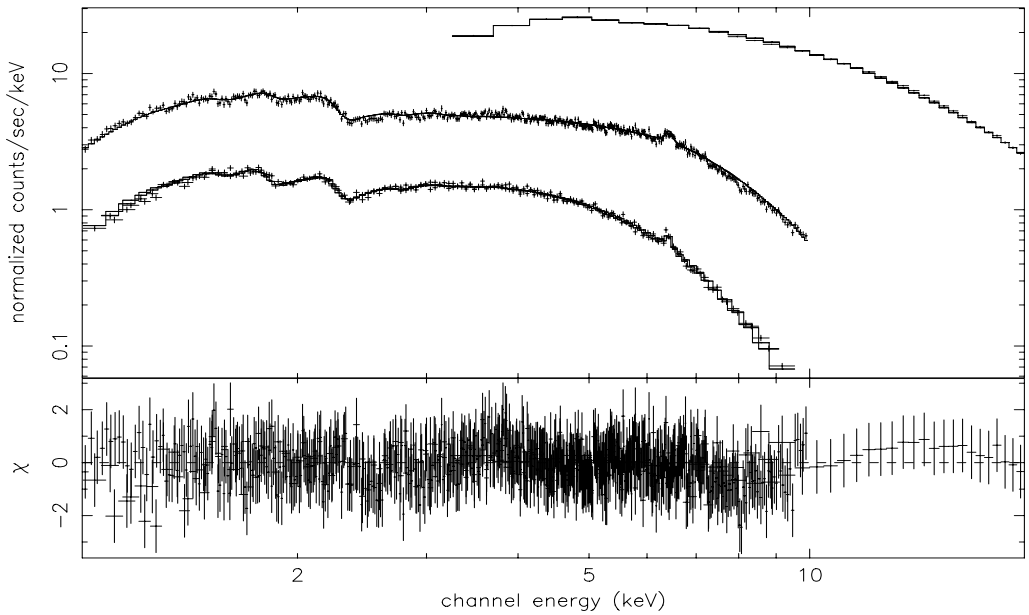

Figure 5.3: 1-20 keV combined PN, MOS1, MOS2 and PCA spectrum of SAX J2103.5+4545 observed on January 6, 2003. The bottom panel shows the residuals of the fit in terms of σ values.

to a luminosity of 7.5×10^{35} ergs s^{-1}. To compare with the average X-ray flux, we found 3-20 keV flux of the January 6 observation to be 6.1×10^{-10} ergs s^{-1} cm^{-2}. This value is approximately 10% greater than the 57.5 days average 3-20 keV RXTE-PCA flux. This is reasonable since the XMM observation took place 3.55 days after the periastron passage where the X-ray flux reaches approximately its maximum (see Fig. 5 and 8 of Baykal et al. 2000b). It should be noted that line parameters obtained from 3-20 keV RXTE PCA data agree with those obtained from XMM EPIC data. However exclusion of the blackbody component, while fitting RXTE PCA data only, increases the absorption column density and equivalent width of line emission and make the power law index harder as shown in Table 5.1, case 4.

To study the spin-phase-resolved spectra using EPIC-PN data, we divided the

Table 5.1: Spectral Models of SAX J2103.5+4545

Parameter	Case 1 **(without BB)**	Case 2 **(with BB)**	Case 3 **(with BB)**	Case 4 **(without BB)**
Multiplication Factors[1] (1.00 for EPIC-PN)				
——MOS 1	0.77 ∓ 0.01	0.76 ∓ 0.01	0.76 ∓ 0.01	na
——MOS 2	0.76 ∓ 0.01	0.75 ∓ 0.01	0.75 ∓ 0.01	na
——PCA	na	na	1.26 ∓ 0.01	na
n_H (10^{22}cm^{-2})	0.90 ∓ 0.02	0.68 ∓ 0.01	0.66 ∓ 0.02	2.98 ∓ 0.14
Iron Line Energy (keV)	6.41 ∓ 0.04	6.42 ∓ 0.02	6.42 ∓ 0.02	6.36 ∓ 0.06
Iron Line Sigma (keV)	0 (fixed)	0 (fixed)	0 (fixed)	0.68 ∓ 0.13
Iron Line Equivalent Width (eV)	48.0 ∓ 7.0	37.1 ∓ 5.3	36.5 ∓ 5.0	107 ∓ 15
Iron Line Flux ($10^{-12}\times$ergs s^{-1} cm^{-2})	1.69 ∓ 0.24	1.37 ∓ 0.20	1.36 ∓ 0.19	5.14 ∓ 0.72
Iron Line Normalization ($10^{-4}\times$photons cm^{-2} s^{-1})	1.65 ∓ 0.24	1.33 ∓ 0.19	1.32 ∓ 0.18	5.00 ∓ 0.70
Blackbody kT (keV)	na	1.91 ∓ 0.04	1.88 ∓ 0.02	na
Blackbody Normalization (km^2 (10kpc)$^{-2}$)	na	0.88 ∓ 0.04	0.83 ∓ 0.07	na
Power Law Index	0.83 ∓ 0.02	0.82 ∓ 0.04	0.77 ∓ 0.05	1.14 ∓ 0.05
Power Law Normalization ($10^{-2}\times$photons keV^{-1} cm^{-2} s^{-1})	1.61 ∓ 0.32	1.03 ∓ 0.26	1.01 ∓ 0.27	3.88 ∓ 0.07
Cut-off Energy (keV)	7.89 (fixed)	7.89 (fixed)	7.89 (fixed)	7.89 (fixed)
E-folding Energy (keV)	27.1 (fixed)	27.1 (fixed)	27.1 (fixed)	27.1 (fixed)
Reduced χ^2	2.69 (1259 d.o.f)	1.23 (1253 d.o.f)	1.11 (1283 d.o.f)	1.20 (30 d.o.f)

[1] **For the cases 1, 2 and 3, we multiplied the entire model with a factor which is varying with the instrument to account for the different normalizations of the instruments (the value of the constant was fixed to be 1 for EPIC-PN).**

spin phase into 10 bins, and fitted 1-10 keV spectrum of each bin with the model including blackbody component (i.e. model in case 3). Figure 4 is a plot of the spectral parameters as a function of the spin phase. For all the spin phases, we found that the model gives an iron line peak energy consistent with 6.42 ± 0.04 keV within 1σ, so we chose to fix this parameter. We also checked the consistence of freezing the cut-off energy, iron line sigma, and e-folding energy parameters, and found that these parameters did not vary significantly when they were thawed. From Figure 4, strong modulation (with a factor of ~ 10) of the blackbody flux with the spin phase is evident. Similarly, the flux of the power law component was shown to be varying with the spin phase, but the variation was more moderate (with a factor of ~ 3) than the that of the blackbody component. The iron line feature at 6.42 keV was stronger for the off-pulse phases where the X-ray flux was lower.

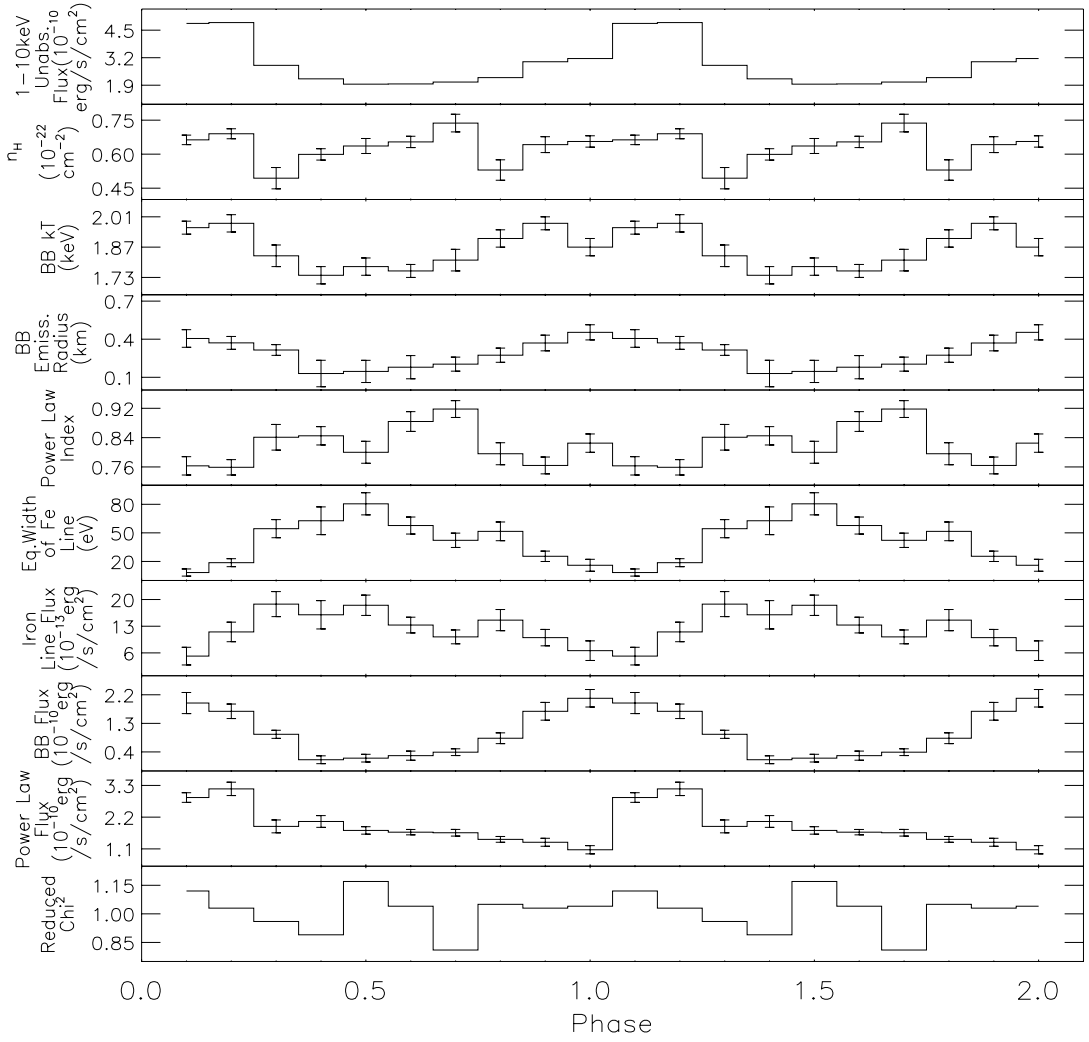

Figure 5.4: Spin phase dependence of 1-10 keV X-ray flux in units of 10^{-10} ergs s^{-1} cm^{-2}, Hydrogen column density in units of 10^{22} cm^{-2}, blackbody kT in units of keV, emission radius of the blackbody (assuming a source distance of 3.2 kpc) in units of km, photon index of the power law component of the spectral model, equivalent width of the iron line in units of eV, flux of the iron line in units of 10^{-13} ergs s^{-1} cm^{-2}, blackbody flux in units of 10^{-10} ergs s^{-1} cm^{-2}, power law flux in units of 10^{-10} ergs s^{-1} cm^{-2}, and reduced χ^2. All of the errors show 1σ confidence level. The spectral model used in fitting consists of an absorbed power law model with high energy cut-off, a soft blackbody component and an Iron line feature modeled as a Gaussian. The values of iron line peak energy, iron line sigma, cut-off and e-folding energies were found to be consistent with the constant values 6.42 keV, 0, 7.89 keV, and 27.1 keV respectively for all the spin phases, so these values were kept fixed while the values of the other model parameters were found.

5.4 Discussion and Conclusion

5.4.1 QPO Feature of SAX J2103.5+4545

Quasi-periodic oscillations in the X-ray band having periods in the range of $\sim 2.5 - 100$s have been observed in many accretion powered X-ray pulsars: 4U 0115+63 (Soong & Swank 1989), EXO 2030+375 (Angelini, Stella,& Parmar 1989), 4U 1626-67 (Shinoda et al. 1990), SMC X-1 (Angelini, Stella,& White 1991), Cen X-3 (Takeshima et al. 1991), V0332+53 (Takeshima et al. 1994), A0535+262 (Finger, Wilson,& Harmon 1996), GRO J1744-28 (Zhang, Morgan,& Jahoda 1996; Kommers et al. 1997), X Per (Takeshima 1997), 4U 1907+09 (in't Zand, Baykal, & Strohmayer 1998; Mukerjee et al. 2001), XTE J1858+034 (Paul & Rao 1998), LMC X-4, and Her X-1 (Moon & Eikenberry 2001a,b). The QPO feature that we found in the XMM-Newton EPIC-PN light curve of SAX J2103.5+4545 which has a peak period of 22.7 ∓ 0.6s and fractional rms amplitude of 6.6 ± 1.9 percent is quite typical (e.g. In't Zand et. al. 1998; Paul & Rao 1998; Takeshima et al. 1994).

Models that explain the QPO phenomenon in accretion powered X-ray pulsars fall basically into three categories: In the Keplerian frequency model, QPOs are produced due to some inhomogeneities at the inner edge of the Keplerian disk (r_0) and modulate the light curve at the Keplerian frequency $\nu_{QPO} = \nu_K$ (van der Klis et al. 1987). In the beat frequency model, the accretion flow onto the neutron star is modulated at the beat frequency between the Keplerian frequency at the inner edge of the accretion disk and the neutron star spin frequency $\nu_{QPO} = \nu_K - \nu_s$

(Alpar & Shaham 1985). The third model involves accretion flow instabilities (Fronter, Lamb,& Miller 1989; Lamb 1988), and applies only to the sources that have luminosities close to Eddington limit, therefore it should not be applicable to our case for which the luminosity is well below the Eddington limit.

In our case, QPO frequency $\nu_{QPO} = 4.4 \times 10^{-2}$Hz is about one order of magnitude greater than the spin frequency $\nu_s = 2.8185 \times 10^{-3}$ Hz. Therefore, it is difficult to distinguish between a Keplerian model and a beat frequency model.

Assuming that the 22.7 s oscillation in SAX J2103.5+4545 is related to Keplerian orbital motion via either Keplerian frequency model or beat frequency model, and using the QPO and its FWHM values we obtain the radius of inner disk as

$$r_0 = \left(\frac{GM}{4\pi^2}\right)^{1/3} \nu_k^{-2/3} = (1.32^{+0.13}_{-0.11}) \times 10^9 \text{cm}, \tag{5.2}$$

where M is 1.4 $M_\odot$ for a neutron star and G is the gravitational constant.

From the strong correlation between pulse frequency derivatives and X-ray flux, Baykal et al. (2002) obtained for the distance to the source 3.2 ± 0.8 kpc and for the magnetic field $(12 \pm 3) \times 10^{12}$ Gauss. Using the distance and magnetic field values, the inner edge of the Keplerian disk r_0 can be found as (Ghosh & Lamb 1979)

$$r_0 \simeq 0.52 \mu^{4/7} (2GM)^{-1/7} \dot{M}^{-2/7} = (1.67^{+0.23}_{-0.25}) \times 10^9 \text{cm}, \tag{5.3}$$

where $\mu = BR^3$ is the neutron star magnetic moment with B the equatorial magnetic field, R the neutron star radius, and $\dot{M}$ the mass accretion rate having the value of $\simeq 4 \times 10^{15}$g s^{-1} for an accretion luminosity of $\simeq 7.5 \times 10^{35}$ erg s^{-1}

(as estimated in Section 3.3).

The radius of the inner disk inferred from the Keplerian orbital motion of inhomogeneities and the one inferred from the Ghosh Lamb disk accretion model agree each other. This shows that the idea that the QPOs are formed due to the Keplerian motion of inhomogeneities is indeed promising as the explanation of the QPO of SAX J2103.5+4545 and the observed QPO frequency is consistent with the distance and the magnetic field values estimated by Baykal et al. (2002).

5.4.2 Blackbody and Iron Line Features of the Energy Spectrum

XMM-Newton observations of SAX J2103.5+4545 revealed for the first time that the energy spectrum of the source has a blackbody component peaking at $\sim$ 1.90keV with the emission radius of $\sim$ 0.3km. The blackbody radiation may come from the polar cap of the neutron star as it appears to for the Be/X-ray pulsar system EXO 2030+375 (Reig & Coe 1999; Sun et al. 1994) and the millisecond X-ray pulsars SAX J1808.4-3658 (Gierlinski, Done,& Didier 2002) and XTE J0920-314 (Juett et al. 2003). Blackbody emission radii on these X-ray pulsars are reported to be greater than $\sim$ 1km. The relatively high surface magnetic field of SAX J2103.5+4545 ($\sim 10^{13}$ Gauss) is probably the reason for the relatively small blackbody emission radius ($\sim$ 0.3 km) compared to these X-ray pulsars. Although the contribution of blackbody component is relatively more significant for lower energies (i.e. energies smaller than $\sim$ 3 keV), power law flux is $\sim$ 3 times greater than the blackbody flux even at the 1-3 keV energy band.

In our case, it is unlikely that the blackbody emission comes from the reprocessed emission of the surrounding material or the accretion disk as in the case of Her X-1 (Endo et al. 2000), Cen X-3 (Burderi et al. 2000), SMC X-1 and LMC X-4 (Paul et al. 2002), since blackbody component in such cases is expected to be softer ($kT \sim 0.1$keV). Lower blackbody temperature and smaller blackbody emission radius at the off-pulse phase shown in Figure 4 are also indications of the plausibility of the polar cap emission interpretation, as the regions of the soft polar cap emission must align with the peak of the X-ray pulse of the pulsar.

Using the spin-phase resolved spectroscopy, strength of the iron line feature at ~ 6.42keV was also found to vary significantly with the spin phase as seen in Figure 4. The peak energy of this feature clearly shows that it corresponds to the fluorescent iron K-line complex. This line complex feature is observed in the spectra of most of the X-ray pulsars (White et al. 1983; Nagase 1989) and is generally thought to be produced by the ions less ionized than Fe XVIII in a relatively cool matter around the neutron star (e.g. accretion disk, accretion disk corona) by fluorescent Kα transition.

Variation of the iron line feature with the spin phase can then be interpreted as a sign that it is mainly produced outside the polar cap region of the neutron star, thus should have a peak at the off-pulse parts of the spin phase. From Figure 4, we see that iron line flux and iron line equivalent width vary strongly with the spin phase, peaking at the off-pulse. Similar pulse phase dependence of the iron line feature is also observed in Her X-1 (Choi et al. 1994).

CHAPTER 6

HER X-1

6.1 Introduction

Her X-1, being an eclipsing accretion powered pulsar consisting of a ~ 1.24 s period pulsar in a ~ 1.7 day circular orbit, was discovered in 1972 using *Uhuru* observations (Tananbaum et al. 1972). Soon after its discovery, its optical companion was identified to be a blue variable thirteenth magnitude star HZ Her (Davidsen al. 1972). The Her X-1/Hz Her binary system was shown to display a 35 day long cycle of high and low X-ray flux states. There are two high states within a single 35 day cycle lasting roughly about 10 and 5 days which are called main high and short high states respectively (Giacconi et al. 1973; Mihara et al. 1991; Scott & Leahy 1999). This 35 day cycle manifests itself with other phenomena including preeclipse X-ray absorption dips that repeat at nearly the beat period of 35 day and 1.7 day (Giacconi et al. 1973; Crosa & Boynton 1980), anomalous dips (Giacconi et al. 1973; Scott & Leahy 1999), optical pulsations occurring at certain 35 day and orbital phases (Middleditch 1983), systematic 35 day variations in the optical light curve (Deeter et al. 1976; Gerend & Boynton 1976), and 35 day X-ray pulse profile evolution (Scott et al. 2000).

In this chapter, December 2001 low state and short high state RXTE-PCA

spectra of Her X-1 are presented Section 2 is an overview about the instruments and the observations. In Section 3, we present the analysis of 2001 December low state and short high observations. In Section 4, results are discussed.

6.2 Instruments and Observations

The RXTE observations used in this paper cover the period from 18 to 26 December 2001 with a total exposure of 281.2 ksec. These observations have common proposal ID 60017. The results presented here are based on data collected with the Proportional Counter Array (PCA, Jahoda et al., 1996). The PCA instrument consists of an array of 5 proportional counters (PCU) operating in the 2-60 keV energy range, with a total effective area of approximately 6250 cm^2 and a field of view of $\sim 1^\circ$ FWHM. Although the number of active PCU's varied between 2 and 5 during the observations, observations in December 2001 (i.e. those with proposal ID 60017) belong to the observational epoch for which background level for one of the PCUs (PCU0) increased due to the fact that this PCU started to operate without a propane layer. The latest combined background models (CM) were used together with FTOOLS 5.2 to estimate the appropriate background.

Spectral analysis and error estimation of the spectral parameters are performed using *XSPEC*. Energy channels corresponding to 3-20 keV energy range are used to fit the spectra. Energies lower than 3 keV are ignored due to uncertainties in background modeling while energies higher than 20 keV are ignored as a result of poor counting statistics. Additional 2% systematic error (see Wilms

Table 6.1: Spectral Parameters of PCA Observations of Her X-1

Parameter	Low State (t=0.34days)	Peak of Short High (t=2.29days)	Anomalous Dip (t=2.51days)	Preeclipse Dip (t=4.85days)
Hydrogen Column Density (10^{22}cm^{-2})	73.5 ∓ 11.8	34.6 ∓ 4.5	69.2 ∓ 2.8	121.1 ∓ 2.9
Partial Cov. Frac.	0.46 ∓ 0.07	0.19 ∓ 0.01	0.83 ∓ 0.04	0.81 ∓ 0.04
Iron Line Energy (keV)	6.72 ∓ 0.04	6.56 ∓ 0.02	6.54 ∓ 0.04	6.81 ∓ 0.03
Iron Line Sigma (keV)	0.34 ∓ 0.09	0.53 ∓ 0.04	1.13 ∓ 0.05	0.74 ∓ 0.03
Iron Normalization ($10^{-3}\times$ cts.cm^{-2}.s^{-1})	0.62 ∓ 0.10	3.67 ∓ 0.27	6.74 ∓ 0.51	1.41 ∓ 0.11
Power Law Normalization ($10^{-2}\times$ cts.keV^{-1}.cm^{-2}.s^{-1})	0.58 ∓ 0.02	5.70 ∓ 0.04	4.11 ∓ 0.06	1.44 ∓ 0.03
3-20 X-ray Flux ($10^{-10}\times$ ergs.cm^{-2}.s^{-1})				
— Absorbed	1.02 ∓ 0.07	14.9 ∓ 0.1	5.54 ∓ 0.08	1.60 ∓ 0.03
— Unabsorbed	1.37 ∓ 0.09	16.3 ∓ 0.1	9.88 ∓ 0.14	3.37 ∓ 0.07
Reduced χ^2 (33 d.o.f)	1.45	0.65	0.66	1.35

et al. 1999; Coburn et al. 2000) is added to the statistical errors.

6.3 Spectral Analysis

2001 December RXTE observation of Her X-1 consists of one low state and four short high state orbits with a total exposure of 281.2 ksec. To investigate the spectral evolution, 111 PCA spectra in 3-20 keV energy range were analyzed.

It is found that the model consisting of an absorbed power law (Morrison & McCammon, 1983) with an high energy cut-off (White, Swank, Holt 1983) and an Iron line feature modeled as a Gaussian was not able to fit the data well . In addition to an overall absorption term we added a partial covering absorption term to the model by multiplying the overall model with the partial covering cold absorber model (pcfabs) in XSPEC. Initially, spectral parameters were determined while keeping all parameters variable. It was found that the overall hydrogen column density, power law photon index, cut-off energy and e-folding energy do not vary considerably throughout the observations, so changes of the values of the other parameters were found keeping overall hydrogen column

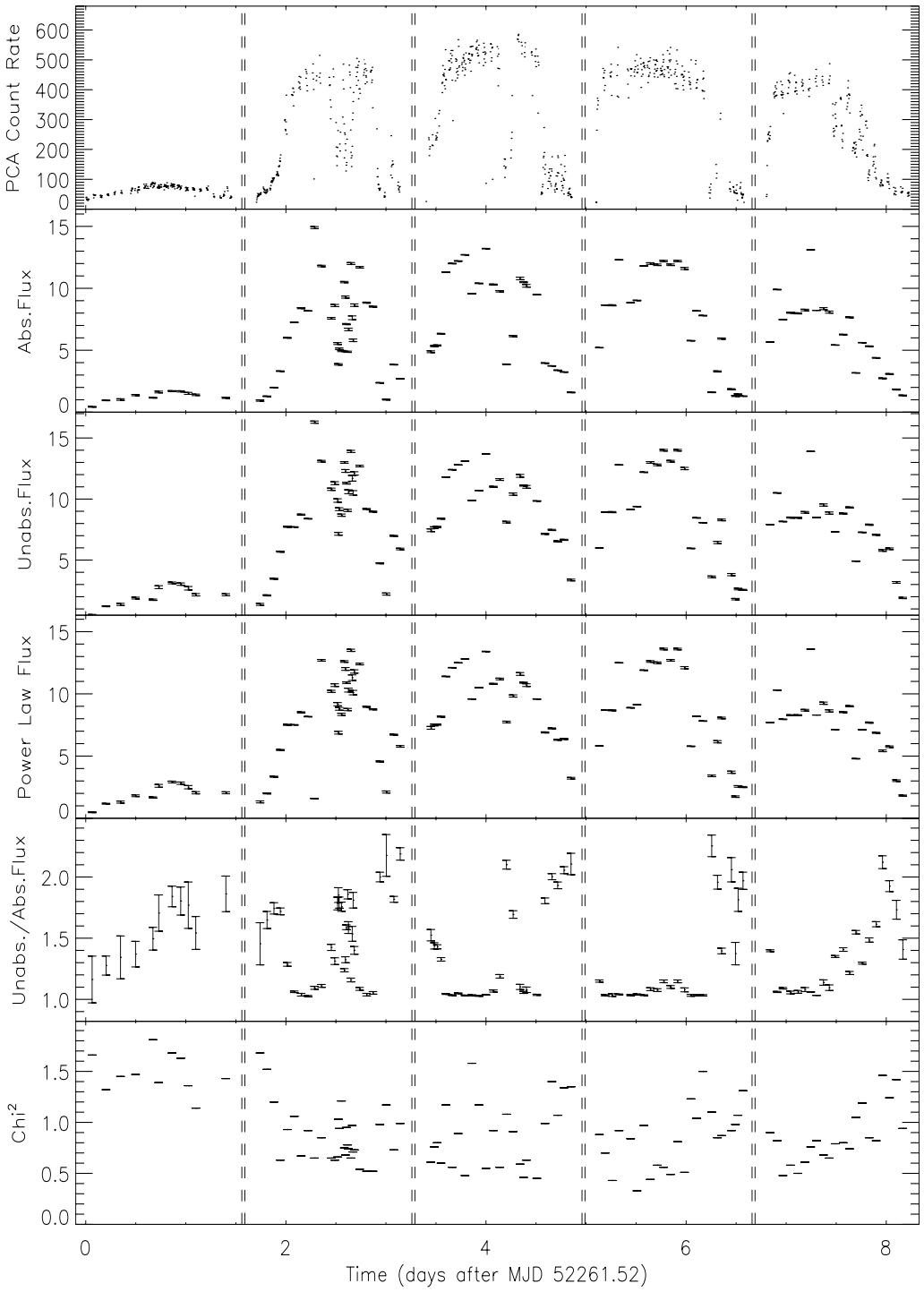

Figure 6.1: PCA count rate in units of cts/s, absorbed flux, unabsorbed flux, and power law flux in units of $10^{-10}\times$ ergs.cm^{-2}.s^{-1} in 3-20 keV energy range, unabsorbed flux / absorbed flux ratio, and reduced χ^2 as a function of time. Errors indicate 1σ confidence.

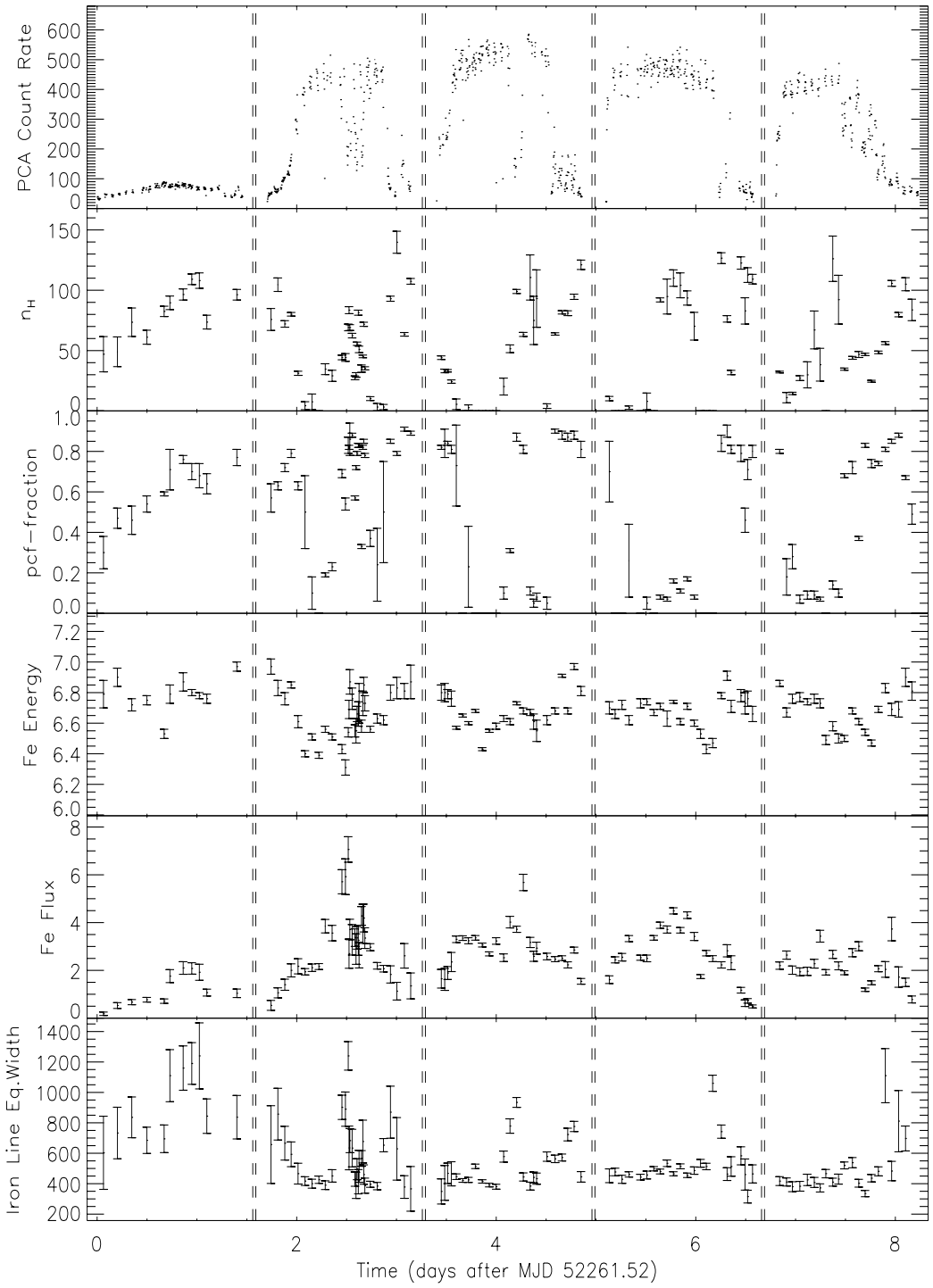

Figure 6.2: PCA count rate in units of cts/s, hydrogen column density in units of 10^{22} cm^2, partial covering fraction, iron line energy in units of keV, iron line flux in units of $10^{-11}\times$ ergs.cm^{-2}.s^{-1}, and iron line equivalent width in units of eV as a function of time. Errors indicate 1σ confidence.

density, power law photon index, cut-off energy and e-folding energy constant with the values 2×10^{22} cm^2, 1.08, 16.8 keV and 20.0 keV respectively.

In Table 6.1, we present sample results of our spectral fits to low state, peak of short high state, anomalous dip and preeclipse dip data. In Figures 6.1 and 6.2, we present evolution of spectral parameters during the low state and short high state orbits.

6.4 Discussion and Conclusion

We analyzed spectra obtained from continuous X-ray monitoring of more than 8 days of Her X-1. Especially continuous monitoring, for the first time, enabled to compare the low state, short high peaks and short high dips within a relatively compact observation period. Having been one of the very well studied sources in X-ray astronomy, this continuous monitoring, although being unique in literature, primarily helped us to confirm the previous spectral results of Her X-1. We would like to make a point the following:

1. As evident from Figure 1, there is a strong correlation of power law flux with the overall flux during both the low state orbit (for which the X-ray flux primarily consists of reflected X-rays coming from the surface of the companion, and thus spectral model should be similar to an high state spectral model but with lower resultant flux; see Coburn et al. 2000) and short high state orbit. This shows that much of the the time independent behavior of Her X-1 is the result of opaque obscuration rather than soft absorption as for July 9-13 short high state of the source (Still et al. 2001). The general increasing trend in each

1.7 day binary orbit of the ratio unabsorbed flux / absorbed flux is evident except for the high flux regions of the short high state where both hydrogen absorption column density and partial covering fraction is low. As opposed to the short high state results of Still et al. 2001, we have not observed a clear anti-correlation of hydrogen column density with the X-ray flux.

2. Evolution of iron line flux and iron line equivalent width shown in Figure 2 shows that strength of the iron line does not vary considerably except for the anomalous dips in the first and second high state orbits. The high values of equivalent width in the third and fourth short high orbits imply a relatively stronger iron line feature with respect the power law continuum, although the iron line flux does not change significantly. Iron line equivalent width is also high in the low state orbits. Strength of the iron line feature in the anomalous dips and preeclipse dips is a natural consequence of the fact that we have part of the X-ray flux coming from the neutron star which is absorbed in low energies while passing through accretion column and/or the edge of the accretion disk which are possibly additional sources of this iron line feature, so that the resultant iron line feature enhances in the dips. Similar low energy absorption in the X-ray spectrum was reported for the main high preeclipse spectrum using TENMA-GSPC (Ushimaru et al. 1989).

CHAPTER 7

CONCLUSION

In this thesis, analysis of *RXTE* and *XMM-Newton* observations of 4U 1907+09, 2S 1417-62 and SAX J2103.5+4545 were presented.

Using X-ray data from *RXTE*, we studied pulse timing of the accretion powered pulsar 4U 1907+09 covering a time span of almost two years. We found three new pulse periods in addition to the previously measured four pulse periods for this system. We were able to connect pulse arrival times in phase for more than a year. The source was found to spin-down in a quite steady rate and residuals of pulse arrival times yielded a very low level of random walk noise strengths. The low level of the timing noise and the very stable spin down rate of 4U 1907+09 makes this source unique among the high mass X-ray binaries, providing another example, in addition to 4U 1626-67, of long term quiet spin down from an accreting source.

As for 2S 1417-62, we analyzed *RXTE* observations between 1999 November and 2000 August with a total exposure of $\sim$ 394 ksec. Observations of this source include a main outburst followed by a series of mini outbursts. Changes in pulse morphology, pulse fraction and X-ray spectrum were found to be related to the changes in X-ray flux. Especially low X-ray flux regions of 2S 1417-62 were found

to have significantly lower pulse fractions with different pulse morphologies. 3-60 keV PCA-HEXTE main outburst spectrum of the source was modeled with an absorbed power law model with high energy cut-off and a Gaussian Iron line complex feature. With the same spectral model, individual 3-20 keV PCA spectra were found to be softer and less absorbed in low X-ray flux regions between outbursts. Spectral studies of 2S 1417-62 showed that hydrogen column density was correlated, and the power law index was anti-correlated with the 3-20 keV X-ray flux. X-ray flux related spectral and timing features in 2S 1417-62 except for low X-ray flux regions were interpreted as a sign of a disc accretion with a similar accretion geometry with a varying mass accretion rate ($\dot{M}$), whereas spectral and timing features of the low X-ray flux regions were interpreted as a sign of possible temporary accretion geometry change prior to the next periastron where $\dot{M}$ increases again to restore the original accretion geometry.

XMM-Newton observed SAX J2103.5+4545 on January 6, 2003, while RXTE was monitoring the source. Using RXTE-PCA dataset between December 3, 2002 and January 29, 2003, we found spin period and average spin-up rate during the XMM-Newton observations as 354.7940 ± 0.0008 s and $(7.4 \pm 0.9) \times 10^{-13}$Hz s^{-1} respectively. In the power spectrum of the 0.9-11 keV EPIC-PN lightcurve, we found a Lorentzian feature corresponding to quasi periodic oscillations around 0.044 Hz (22.7 s) with an rms fractional amplitude $\sim$6.6 %. This QPO feature of this source was interpreted as the Keplerian motion of inhomogenuities through the inner disk. In the X-ray spectrum, in addition to the power law component model with high energy cutoff and $\sim$ 6.4 keV fluorescent iron emission line which

was the model used by Baykal et al. (2002), we discovered a soft component consistent with a blackbody emission with kT $\sim$ 1.9keV. The pulse phase spectroscopy of the source revealed that the blackbody flux peaked at the peak of the pulse with an emission radius $\sim$ 0.3 km, suggesting the polar cap on the neutron star surface as the source of blackbody emission. The flux of the iron emission line at $\sim$ 6.42 keV was shown to peak at the off-pulse phase, supporting the idea that this feature arises from fluorescent emission of the circumstellar material around the neutron star rather than the hot region in the vicinity of the neutron star polar cap.

We also analyzed spectral variations of $\sim$ 8 days December 2001 RXTE monitoring observations of Her X-1 covering one low state and four short high state orbits. These observations enabled, for the first time, to continuosly analyze the spectral evolution of the source from the last orbit of a low state till the end of the fourth orbit of a short high state. Power law model with partial cold absorber was found to be the appropriate spectral model. Opaque obscuration of the pulsar beam was thought to be primary reason for the X-ray flux changes. The strength of the iron line feature at $\sim$ 6.5 keV was found to be significantly higher for the anomalous dips. This feature was also found to be relatively high in the preeclipse dips and low state orbits. The reason for stronger iron line feature in the anomalous dips and preeclipse dips were discussed to be due to the partially covering matter in the line of sight (edge of the accretion disk or accretion column). Iron line flux was found to be not varying significantly for the rest of the observations.

REFERENCES

[1] Alpar, M.A., Shaham, J. 1985, "Is GX 5-1 a Millisecond Pulsar", Nature, 316, 239

[2] Angelini, L., Stella, L., Parmar, A.N. 1989, "The Discovery of 0.2 Hz Quasi-periodic Oscillations in the X-ray Flux of the Transient 42 Second Pulsar EXO 2030+375", ApJ, 346, 906

[3] Angelini, L., Stella, L., White, N.E. 1991, "The Discovery of an X-ray Burst and a Study of Aperiodic Variability from SMC X-1", ApJ, 371, 332

[4] Apparao, K.M.V. et al. 1980, "2S 1417-624 - A Variable X-ray Source near CG312-1", A&A, 89, 249

[5] Basko, M.M., Sunyaey, R.A. 1976, "The Limiting Luminosity of Accreting Neutron Stars with Magnetic Fields", MNRAS, 175, 395

[6] Baykal, A., Swank, J., 1996, "Pulse Frequency Changes of 1E 2259+586 and the Binary Interpretation", ApJ, 460, 470

[7] Baykal, A., Stark, M., Swank, J., 2000a, "SAX J2103.5+4545", IAU Circ. 7355

[8] Baykal, A., Stark, M., Swank, J., 2000b, "Discovery of the Orbit of the Transient X-ray Pulsar SAX J2103.5+4545", ApJL, 544, 129

[9] Baykal, A. et al. 2001, "The Steady Spin-down Rate of 4U 1907+09", MNRAS, 327, 1269

[10] Baykal, A. et al. 2002, "X-ray Spectra and Pulse Frequency Changes in SAX J2103.5+4545", ApJ, 569, 903

[11] Baykal, A. et al. 2004, in preparation

[12] Bildsten, L. et al. 1997, "Observations of Accreting Pulsars", ApJS., 113, 367

[13] Blondin, J.M. et al. 1990, "Hydrodynamic simulations of stellar wind disruption by a compact X-ray source", ApJ, 356, 591

[14] Boynton, P.E., 1981, "Pulse timing and neutron star structure", in Pulsar, IAU Symposium No.95, ed W.Sieber and R. Wielebinski, (Dordrecht: Reidel), 279

[15] Bulik, T. et al. 1992, "The Polar Cap Structure of the X-ray Pulsar 4U 1538 - 52", ApJ, 395, 564

[16] Bulik, T. et al. 2003, "A Puzzling Paucity of Double Peaked X-ray Pulsars", A&A, 404, 1023

[17] Burderi, L. et al. 2000, "The 0.1-100 keV Spectrum of Centaurus X-3: Pulse Phase Spectroscopy of the Cyclotron Line and Magnetic Field Structure", ApJ., 530, 429

[18] Campana, S. et al. 1998, "Aquila X-1 from Outburst to Quiescence: The Onset of the Propeller Effect and Signs of a Turned-on Rotation-powered Pulsar", ApJL, 499, 65

[19] Campana, S. et al. 2002, "The Quiescent X-Ray Emission of Three Transient X-Ray Pulsars", ApJ, 580, 389

[20] Canuto, V., Lodenquai, J., Ruderman, M. 1971, "Thomson Scattering in a Strong Magnetic Field", Phys. Rev. D., 3, 2303

[21] Chakrabarty, D. 1996, "Hard X-Ray Detection and Timing of Accretion-Powered Pulsars with BATSE", PhDT, California Institute of Technology

[22] Chakrabarty, D. et al. 1997, "Torque Reversal and Spin-down of the Accretion-powered Pulsar 4U 1626-67", ApJ, 474,414

[23] Choi, C.S., Nagase, F., Makino, F., 1994, "Iron Line Intensity Variations of Hercules X-1 over the Pulse Phase and the 35 Day Cycle", ApJ, 437, 449

[24] Coburn, W. et al. 2000, "The 1999 Hercules X-1 Anomalous Low State", ApJ, 543, 351

[25] Coburn, W. et. al. 2002, "Magnetic Fields of Accreting X-ray Pulsars with the Rossi X-ray Timing Explorer", ApJ., 580, 394

[26] Cook, M.C., Page, C.G., 1987, "The X-ray Properties of 3A1907 + 09", MNRAS, 225, 381

[27] Corbet, R.H.D. 1986, "The Three Types of High-mass X-ray Pulsator", MNRAS, 220, 1047

[28] Corbet, R.H.D., 1996, "Transient X-Ray Sources, Luminosity Gaps, and Neutron Star Densities", ApJL, 457, 31

[29] Cordes, J.M., 1980, "Pulsar Timing. II - Analysis of Random Walk Timing Noise - Application to the Crab Pulsar", ApJ, 237, 216

[30] Crosa L., Boynton P.E., 1980, "Periodic Mass Transfer in Hercules X-1/HZ Herculis", ApJ, 235, 999

[31] Cui, W., 1997, "Evidence for 'Propeller' Effects in X-Ray Pulsars GX 1+4 and GRO J1744-28", ApJL, 482, 163

[32] Cusumano, G. et al. 1998, "Detection of a Cyclotron Line and its Second Harmonic in 4U1907+09", A&AL, 338, 79

[33] Davidsen, A. et al. 1972, "Identification of the X-Ray Pulsar in Hercules: a New Optical Pulsar", ApJL, 177, 97

[34] Deeter J. et al. 1976, "Analysis of Periodic Optical Variability in the Compact X-ray Source HER X-1/HZ Herculis", ApJ, 206, 861

[35] Deeter, J.E., Boynton, P.E., 1982, "Techniques for the estimation of red power spectra. I - Context and methodology", ApJ, 261, 337

[36] Deeter, J.E., 1984, "Techniques for the Estimation of Red Power Spectra. II Evaluation of Alternative Methods", ApJ, 281, 482

[37] Deeter, J.E. et al. 1989, "Vela X-1 Pulse Timing. II - Variations in Pulse Frequency", ApJ, 336,376

[38] Endo, T., Nagase, F., Mihara, T., 2000, "Pulse-Phase Resolved Spectroscopy of Hercules X-1 with ASCA", AdSpR, 25, 421

[39] Erkoca, A., 2004, "The Red Noise Power Density Estimation Techniques and Application to the Source SAX J2103.5+4545", M.S. Thesis, Middle East Technical University

[40] Finger, M.H., Wilson, R.B., Chakrabarty, D., 1996, "Reappearance of the X-ray Binary Pulsar 2S 1417-624", A&AS, 120, 209

[41] Finger, M.H., Wilson, R.B., Harmon, B.A., 1996, "Quasi-Periodic Oscillations during a Giant Outburst of A0535+262", ApJ, 459, 288

[42] Finger, M.H. et al. 1999, "The Outbursts and Orbit of the Accreting Pulsar GS 1843-02=2s 1845-024", ApJ, 517, 449

[43] Fronter, B., Lamb, F.K., Miller, G.S. 1989, "Origin of 'Normal-branch' Quasiperiodic Oscillations in Low-mass X-ray Binary Systems", Nature, 342, 775

[44] Galloway, D., Morgan, E., Levine, W., 2004, "A Frequency Glitch in an Accreting Pulsar", ApJ, 613, 1164

[45] Gerend D., Boynton P.E., 1976, "Optical Clues to the Nature of Hercules X-1/HZ Herculis", ApJ, 209, 562

[46] Ghosh, P., 1993, "Spin Evolution of Neutron Stars in Accretion Powered Pulsars", in Holt S.S., Day, C.S., ed, The Evolution of X-ray Binaries. Am. Inst. Phys., New York, 439

[47] Ghosh, P., Lamb, F.K., 1979a, "Accretion by Rotating Magnetic Neutron Stars. II - Radial and Vertical Structure of the Transition Zone in Disk Accretion", ApJ, 232, 259

[48] Ghosh, P., Lamb, F.K., 1979b, "Accretion by Rotating Magnetic Neutron Stars. III. Accretion Torques and Period Changes in Pulsating X-ray Sources", ApJ., 234, 296

[49] Giacconi, R. et al. 1971a, "An X-Ray Scan of the Galactic Plane from UHURU", ApJL, 165, 27

[50] Giacconi, R. et al. 1971b, "Discovery of Periodic X-ray Pulsations in Centaurus X-3 from Uhuru", ApJL, 167, 67

[51] Giacconi R. et al. 1973, "Further X-ray Observations of Her X-1 from Uhuru", ApJ, 184, 227

[52] Gierlinski, M., Done, C., Didier, B., 2002, "Phase Resolved X-ray Spectroscopy of the Millisecond Pulsar SAX J1808.4+3658", MNRAS, 331, 141

[53] Grindlay, J.E., Petro, L.D., McClintock, J.E., 1984, "Optical Identification of 2S 1417-62", ApJ, 276,621

[54] Harding, A.K. et al. 1984, "Self-consistent Models for Coulomb-Heated X-ray Pulsar Atmospheres", ApJ, 278, 369

[55] Hewish, A. et al. 1968, "Observation of a Rapidly Pulsating Radio Source", Nature, 217, 709

[56] Hullemann, F., in't Zand, J.J.M., Heise, J., 1998, "Discovery of the Transient X-ray Pulsar SAX J2103.5+4545", A&AL, 337, 25

[57] Illarionov, A.F., Sunyaev, R.A., 1975, "Why the Number of Galactic X-ray Stars Is so Small?", A&A, 39, 185

[58] Inam, S.C., Baykal, A., 2000, "X-ray Flux and Pulse Frequency Changes of Three High Mass X-ray Binary Pulsars: Vela X-1, GX 301-2 and OAO 1657-415", A&A, 353, 617

[59] Inam, S.C. et al. 2004a, "X-ray Flux Related Timing and Spectral Features of 2S 1417-62", MNRAS, 349, 173

[60] Inam, S.C. et al. 2004b, "Discovery of a Soft Spectral Component and Transient 22.7 second Quasi-periodic Oscillations of SAX J2103.5+4545", Accepted for publication in ApJ

[61] in't Zand, J.J.M., Strohmayer, T.E., Baykal, A., 1997, "Dipping Activity in the X-Ray Pulsar 4U 1907+09", ApJL, 479, 47

[62] in't Zand, J.J.M., Corbet, R.H.D., Marshall, F.E., 2001, "Discovery of a 75 Day Orbit in XTE J1543-568", ApJL, 533, 165

[63] in't Zand, J.J.M., Baykal, A., Strohmayer, T.E. 1998a, "Recent X-Ray Measurements of the Accretion-powered Pulsar 4U 1907+09", ApJ, 496, 386

[64] in't Zand, J.J.M., Strohmayer, T.E., Baykal, A. 1998b, "Spin down and oscillations in 4U 1907+09: a retrograde disk?", Nucl.Phys.B., 69, 224

[65] Jahoda, K. et al. 1996, "In-orbit performance and calibration of the Rossi X-ray Timing Explorer (RXTE) Proportional Counter Array (PCA)", Proc. SPIE, 2808, 59

[66] Juett, A.M., Galloway, D.K., Chakrabarty, D., 2003, "X-ray Spectroscopy of the Accreting Millisecond Pulsar XTE J0929-314 in Outburst", ApJ, 587, 754

[67] Kaspi, V.M., Chakrabarty, D., Steinberger, J., 1999, "Precision Timing of Two Anomalous X-Ray Pulsars", ApJL, 525, 33

[68] Kelley, R.L et al. 1981, "Discovery of X-ray Pulsations from 2S 1417-624", ApJ, 243, 251

[69] Kommers, J.M. et al. 1997, "Postburst Quasi-periodic Oscillations from GRO J1744-28 and from the Rapid Burster", ApJL, 482, 53

[70] Kouveliotou, C. et al. 1996, "A New Type of Transient High-energy Source in the Direction of the Galactic Centre", Nature, 379, 799

[71] Lamb, F.K., Pines, D., Shaham, J., 1978a, "Period Variations in Pulsating X-ray Sources. I - Accretion Flow Parameters and Neutron Star Structure from Timing Observations", ApJ, 224, 969

[72] Lamb, F.K., Pines, D., Shaham, J., 1978b, "Period Variations in Pulsating X-ray Sources. II - Torque Variations and Stellar Response", ApJ, 225, 582

[73] Lamb, F.K. 1988, "Models of QPOs in Luminous Low-mass X-ray Binaries", Adv. Space Res., 8, 421

[74] Lamb, F.K., 1989, "Accretion by Magnetic Neutron Stars", Timing Neutron Stars, ed. H. Ögelman, E.P.J. van den Heuvel (Dordrecht, Kluwer), 649

[75] Lamb, F.K., 1991, "Neutron Stars and Black Holes", Frontiers of Stellar Evolution, ed by D.L.Lambert (Astronomical Society of the Pacific), 299-388

[76] Leahy, D.A. et al. 1983, "On Searches for Pulsed Emission with Application to four Globular Cluster X-ray Sources - NGC 1851, 6441, 6624, and 6712", ApJ, 266,160

[77] Levine, A.M., Rappaport, A., Zojcheski, G., 2000, "Orbital Decay in LMC X-4", ApJ, 541, 194

[78] Lutovinov, A.A., Molkov, S.V., Revnivtsev, M.G., 2003, "The First Results of Observations of the Transient Pulsar SAX J2103.5+4545 by the INTEGRAL Observatory", Astron. Lett., 29, 713

[79] Makishima, K. et al. 1984, "Discovery of a 437.5-s X-ray Pulsation from 4U 1907+09", PASJ, 36,679

[80] Makishima, K. et al. 1987, "Spectra and Pulse Period of the Binary X-ray Pulsar 4U 1538-52", ApJ, 314,619

[81] Makishima, K., Mihara, T., 1992, "Magnetic Fields of Neutron Stars", in Tanaka Y., Koyama K. eds. Proc. XXVIII Yamada Conf., Frontiers of X-ray Astronomy. Universal Academy Press, Tokyo, 23

[82] Marshall, N., Rickets, M.J., 1980, "Determination of a Binary Period for the Variable X-ray Source A1907+09", MNRAS, 193, 7

[83] Meszaros, P. et al. 1983, "Accreting X-ray Pulsar Atmospheres Heated by Coulomb Deceleration of Protons", ApJL, 266, 33

[84] Meszaros, P., 1992, High Energy Radiation from Magnetized Neutron Stars (Chicago, Univ. Chicago Press)

[85] Middleditch J. 1983, "Optical pulsations from HZ Herculis/Hercules X-1 - The self-consistent 35 day picture", ApJ, 275, 278

[86] Mihara, T. et al. 1991, "X-ray Spectrum of Hercules X-1 in the Low State of the 35-day Cycle", PASJ, 43, 501

[87] Mihara, T., 1995, "Observational Study of X-ray Spectra of Binary Pulsars with Ginga", PhDT, Dept. of Physics, Univ. of Tokyo

[88] Moon, D., Eikenberry, S.S. 2001a, "Large X-ray Flares from LMC X-4: Discovery of Millihertz Quasi-periodic Oscillations and Quasi-periodic Oscillation-Modulated Pulsations", ApJL, 549, 225

[89] Moon, D., Eikenberry, S.S. 2001b, "Discovery of Coupling between Periodic and Aperiodic Variability and X-ray Quasi-periodic Oscillations from Hercules X-1", ApJL, 552, 135

[90] Morrison, R., McCammon, D., 1983, "Interstellar Photoelectric Absorption Cross Sections, 0.03-10 keV", ApJ, 270, 119

[91] Mukerjee, K. et al. 2001, "Pulse Characteristics of the X-ray Pulsar 4U 1907+09", ApJ, 548, 368

[92] Nagase, F., 1989, "Accretion Powered X-ray Pulsars", PASJ., 41, 1

[93] Negueruela, I., 1998, "On the Nature of Be/X-ray Binaries", A&A, 338, 505

[94] Negueruela, I. et al. 1989, "A Model for Compact X-Ray Sources: Accretion by Rotating Magnetic Stars", ApJ, 184, 271

[95] Parmar, A.N., White, N.E., Stella, L. 1989, "The Transient 42 second X-ray Pulsar EXO 2030+375. II - The Luminosity Dependence of the Pulse Profile", ApJ, 338, 373

[96] Parmar, A.N. et al. 1989, "The Transient 42 second X-ray Pulsar EXO 2030+375. I - The Discovery and the Luminosity Dependence of the Pulse Period Variations", ApJ, 338, 359

[97] Paul, B. et al. 2002, "Nature of the Soft Spectral Component in the X-ray Pulsars SMC X-1 and LMC X-4", ApJ, 579, 411

[98] Paul, B., Rao, A.R. 1998, "Quasi-periodic Oscillations Discovered in the New X-ray Pulsar XTE J1858+034", A& A, 337, 815

[99] Reig, P., Coe, M.J., 1999, "X-ray Spectral Properties of the Pulsar EXO 2030+375 during an Outburst", MNRAS, 302, 700

[100] Reig, P., Mavromatakis, F., 2003, "The Optical Counterpart to the Transient X-ray Pulsar SAX J2103.5+4545", Astron. Telegram, 173, 1

[101] Rice. S.O., 1954, Selected Papers on Noise and Stochastic Processes. Wax N. (ed), Dover, London, p.133

[102] Robba, N.R. et al. 1992, "EXOSAT Observations of the X-ray Binary Pulsar 4U 1538-52", ApJ, 401, 685

[103] Rothschild, R.E. et al. 1998, "In-Flight Performance of the High-Energy X-Ray Timing Experiment on the Rossi X-Ray Timing Explorer", ApJ, 496, 538

[104] Robba, N.R., Cusumona, G., Orlandini, M. et al. 1992, "EXOSAT Observations of the X-ray Binary Pulsar 4U 1538-52", ApJ, 401, 685

[105] Schreier, E. et al. 1972, "Evidence for the Binary Nature of Centaurus X-3 from UHURU X-Ray Observations", ApJL, 172, 79

[106] Scott, D.M. et al. 1997, "Discovery and Orbital Determination of the Transient X-Ray Pulsar GRO J1750-27", ApJ, 488, 831

[107] Scott D.M., Leahy D.A., Wilson R.B., 2000, "The 35 Day Evolution of the Hercules X-1 Pulse Profile: Evidence for a Resolved Inner Disk Occultation of the Neutron Star", ApJ, 539, 392

[108] Scott, D.M., Finger, M.H., Wilson, C.A., 2003, "Characterization of the Timing Noise of the Crab Pulsar", MNRAS, 344, 412

[109] Shinoda, K., Kii, T., Mitsuda, K. 1990, "Discovery of the Quasi-periodic Oscillations from the X-ray Pulsar X1627-673", PASJL, 42, 27

[110] Slettebak, A., 1988, "The Be Stars", PASP, 100, 770

[111] Soong, Y., Swank, J., 1989, "Timing analysis of binary X ray pulsars observed by HEAO 1", in Proc. 23d ESLAB Symp., Two Topics in X-ray Astronomy, Vol. 1, ed. N. White (Garching: ESA), 617

[112] Stark, M.J. et al. 1996, "Pulse Arrival Time Glitches in GRO J1744-28", ApJL, 470, 109

[113] Stella, L., White, N.E., Rosner, R., 1986, "Intermittent Stellar Wind Accretion and the Long-term Activity of Population I Binary Systems Containing an X-ray pulsar", ApJ, 308, 669

[114] Still M., O'Brien K., Horne K. et al. 2001, "RXTE Observations of Hercules X-1 during the 1998 July Short High State", ApJ, 553, 776

[115] Struder, L. et al. 2001, "The European Photon Imaging Camera on XMM-Newton: The pn-CCD camera", A&AL, 365, 18

[116] Sun, X.-J. et al. 1994, "The X-ray Spectrum of EXO 2030+375", A&A, 289, 127

[117] Taam, R.E., Fryxell, B.A., 1988, "On Nonsteady Accretion in Stellar Wind-fed X-ray Sources", ApJL, 327, 73

[118] Taam, R.E., Fryxell, B.A., 1989, "A study of some Southern Planetary Nebulae", ApJ, 334, 862

[119] Takeshima, T., Dotani, T., Mitsuda, K. et al. 1991, "Quasi-periodic oscillations in the X-ray flux from Centaurus X-3 observed with GINGA", PASJL, 43, 43

[120] Takeshima, T., Dotani, T., Mitsuda, K. et al. 1994, "Discovery of the Quasi-periodic Oscillations from V0332+53", ApJ, 436, 871

[121] Takeshima, T. 1997, "Discovery of Quasi-Periodic Oscillations from X Persei", BAAS, 19111104

[122] Tannanbaum, H. et al. 1972, "Discovery of a Periodic Pulsating Binary X-Ray Source in Hercules from UHURU", ApJL, 174, 143

[123] Thompson, C., Duncan, R.C., 1993, "Neutron Star Dynamos and the Origins of Pulsar Magnetism", ApJ, 408, 194

[124] Trümper, J. et al. 1978, "Evidence for Strong Cyclotron Line Emission in the Hard X-ray Spectrum of Hercules X-1", ApJL, 219, 105

[125] Turner, M.J.L. et al. 2001, "The European Photon Imaging Camera on XMM-Newton: The MOS Cameras", A&AL, 365, 27

[126] Ushimaru, N. et al. 1989, "Energy Spectra and Pulse Profiles of Hercules X-1 at Pre-eclipse Dips", PASJ, 41 441

[127] Valinia, A., Marshall, F.E., 1998, "RXTE Measurement of the Diffuse X-Ray Emission from the Galactic Ridge: Implications for the Energetics of the Interstellar Medium", ApJ, 505, 134

[128] van der Klis, M. et al. 1987, "Intensity and Source State Dependence of the Quasi-periodic Oscillations in Scorpius X-1", ApJ, 316, 411

[129] van der Klis, M., 1989, "Quasi-periodic Oscillations and Noise in Low-mass X-ray Binaries", in Timing Neutron Stars, ed. H.Ogelman & E.P.J. van den Heuvel (Dordrecht:Kluwer), 27

[130] van Kerkwijk, M.H., Chakrabarty, D., Pringle, J.E., Wijers, R.A.M.J., 1998, "Warped Disks as a Possible Origin of Torque Reversals in Accretion-powered Pulsars", ApJL, 499, 27

[131] Wang, Y.-M., Frank, J. 1981, "Plasma Infall and X-ray Production in the Magnetic Funnel of an Accreting Neutron Star", A&A, 93, 255

[132] Waters, L.B.F.M., van Kerkwijk, M.H. 1989, "The Relation between Orbital and Spin Periods in Massive X-ray Binaries", A& A,223, 196

[133] White, N.E., Swank, J.H., Holt, S.S. 1983, "Accretion Powered X-ray Pulsars", ApJ, 270, 711

[134] Wilms, J. et al. 1999, "Low-Luminosity States of the Black Hole Candidate GX 339-4. I. ASCA and Simultaneous Radio/RXTE Observations", ApJ, 522, 460

[135] Wilson, C.A. et al. 2002, "A Decade in the Life of EXO 2030+375: A Multiwavelength Study of an Accreting X-Ray Pulsar", ApJ, 570, 287

[136] Zeldovich, Y.B., Guseinov, O.H., 1966, "Collapsed Stars in Binaries", ApJL, 144, 840

[137] Zhang, W., Morgan, E.H., Jahoda, K. 1996, "Quasi-periodic X-Ray Brightness Oscillations of GRO J1744-28", ApJL, 469, 29

[138] Zhang, Z.N., Yu, W., Zhang, W., 1998, "Spectral Transitions in Aquila X-1: Evidence for 'Propeller' Effects", ApJL, 494, 71

VITA

Sıtkı Çağdaş İnam was born in İstanbul on January 18, 1975. He received his B.S and M.S degrees in Physics from the Middle East Technical University in 1997 and 1999 respectively. He worked in Physics Department of the Middle East Technical University from 1997 to 2004. Meanwhile, he visited National Space Science and Technology Center in Huntsville, Alabama, USA from 2001 to 2002 as a visiting scholar. His main area of interest is high energy astrophysics.